Ccn2a-FGFR1-SHH Signaling is Necessary for Intervertebral Disc Homeostasis and Regeneration in Adult Zebrafish

Amey Y. Rayrikar[1,2], Ganesh A. Wagh[1,2], Manas Santra[3], and Chinmoy Patra[1,2,*]

[1]Department of Developmental Biology, Agharkar Research Institute, Pune, Maharashtra, 411004, India
[2]S P Pune University, Pune, Maharashtra, 411007, India
[3]National Centre for Cell Science, Pune, Maharashtra, 411007, India

[*]Corresponding author: Chinmoy Patra, PhD, Scientist E
DBT/Wellcome Trust IA Intermediate fellow, Developmental Biology group
Agharkar Research Institute, Pune – 411004, Maharashtra, India.
Tel.: +91-2532-5046, Fax: +91-2565-1542
E-mail: cpatra@aripune.org

Keywords: Intervertebral disc; CCN2; zebrafish; regeneration; FGFR; SHH

Abstract

Intervertebral disc (IVD) degeneration is the primary cause of back pain in humans. However, the cellular and molecular pathogenesis of IVD degeneration is poorly understood. This study shows that zebrafish IVDs possess distinct and non-overlapping zones of cell proliferation and cell death. We find that in zebrafish, *cellular communication network factor 2a* (*ccn2a*) is expressed in notochord and IVDs. Although IVD development appears normal in *ccn2a* mutants, the adult mutant IVDs exhibit decreased cell proliferation and increased cell death leading to IVD degeneration. Moreover, Ccn2a overexpression promotes regeneration through accelerating cell proliferation and suppressing cell death in wild-type aged IVDs. Mechanistically, Ccn2a maintains IVD homeostasis and promotes IVD regeneration by enhancing outer annulus fibrosus cell proliferation and suppressing nucleus pulposus cell death through augmenting FGFR1-SHH signaling. These findings reveal that Ccn2a plays a central role in IVD homeostasis and regeneration, which could be exploited for therapeutic intervention in degenerated human discs.

Introduction

Intervertebral disc (IVD), a fibrocartilaginous tissue placed between adjacent vertebrae, is present in all vertebrates. In mammals, including humans, IVD consists of centrally placed large vacuolated notochordal cell (NC) populated nucleus pulposus (NP), which is encapsulated by annulus fibrosus (AF), a multilayered angularly arranged lamellar collagenous structure consisting of fibroblasts (Hashizume, 1980). Further, AF is subdivided into two zones; outer annulus fibrosus (OAF), made up of small, tightly packed cells and inner annulus fibrosus (IAF), made up of elongated cells (Rufai et al., 1995).

IVD degeneration (IVDD) is considered a major reason for back, neck, and appendage pain, putting a considerable socio-economic burden on the clinical system (Cheung et al., 2009). Historically, disc degeneration was believed to be associated only with aging (Buckwalter, 1995); however, recent studies suggest that it is also linked to genetic (Eskola et al., 2010) and health-related (Teraguchi et al., 2017) backgrounds. Physical analysis of human discs has shown that IVDD starts from the NP region (Pearce et al., 1987). However, molecular and cellular mechanisms involved in IVD homeostasis and degeneration are poorly understood. Irrespective of the reason, alterations in extracellular matrix (ECM) composition and cell morphology are visible in degenerating discs (Roughley, 2004). Thus, understanding the role and working cascades of ECM molecules in IVD maintenance and regeneration will help develop therapeutic strategies to counter IVDD.

Cellular communication network factor 2 (*CCN2*), an ECM molecule, plays a role in the progression of fibrotic diseases (Jaffa et al., 2008; Mori et al., 1999; Tamatani et al., 1998) as well as in tissue regeneration (Mokalled et al., 2016; Mukherjee et al., 2021; Riley et al., 2015) in a context and tissue microenvironment-dependent manner. In mice, notochord-specific deletion of *Ccn2* leads to an early onset of IVDD (Bedore et al., 2013). An *in vitro* study showed that the combinatorial application of TGF-β1 and CCN2 promotes rat tail disc-derived NP cell survival (Matta et al., 2017). On the contrary, Wu et al. have suggested that TGFβ induced CCN2 secretion leads to notochordal cell death *in vitro* (Wu et al., 2019). Thus, the cellular and molecular functions of CCN2 in IVDD remain to be explored.

In this study, we sought to explore the role of Ccn2a, a zebrafish orthologue of human CCN2, in IVD homeostasis and regeneration in zebrafish. Histology revealed that cellular morphology and arrangement in zebrafish IVDs is similar to mammalian counterpart. We

find that *ccn2a* expresses in adult IVDs. Although *ccn2a* mutants are viable adults, *ccn2a*$^{-/-}$ IVDs show diminished cell proliferation and survival at 4 months post-fertilization (mpf), leading to an early onset of IVDD. Interestingly, in aged degenerated IVDs, ectopic expression of Ccn2a promotes OAF cell proliferation and NP cell survival. Through genetic and biochemical approaches, our findings reveal that Ccn2a maintains the cell turnover in adult IVDs and can induce regeneration in degenerated IVDs by augmenting FGFR1-SHH signaling. This study enriches our understanding of the cellular and molecular mechanisms through which Ccn2a maintains IVD homeostasis and its potential therapeutic implications to promote regeneration in degenerated human discs.

Results

Morphologically adult zebrafish IVD is homologous to the mammalian counterpart

Although a handful of evidence is available about chordacentra morphogenesis (Haga et al., 2009; Lleras Forero et al., 2018; Wopat et al., 2018), the cellular arrangement in adult zebrafish IVDs remains to be learned. Our histological analysis identified, at 12 days post fertilization (dpf) (~6 mm length), notochordal sheath cells (NSCs) from the junctional area of adjacent chordacentra (future IVD forming region) protrude into the notochordal cell zone (Fig. S1 A and B). At 20 dpf (~8 mm length), sagittal sections through the intervertebral region showed three distinct types of cellular arrangements, viz. outermost tightly packed one-layer of small cells, followed by one-two layer of elongated cells arranged in parallel with the spine and innermost large cells (Fig. S1 C and C'). The number of layers of small cells in the outermost compact zone and elongated cells in the adjacent zone increase with the progression of age towards adulthood (Fig. S1 D and D'). Based on the similarity of cellular morphology and arrangements between adult mammals and zebrafish, we named the outermost area covered by 3-4 layers of compact cells as outer annulus fibrosus (OAF), the adjacent area filled with 4-5 layers of elongated cells as inner annulus fibrosus (IAF), and innermost region filled with large cells as nucleus pulposus (NP) (Fig. S1 D and D'). IVDs and the tissue connecting IVDs are covered with a monolayer of epithelial-like cells, presumably the NSCs (Fig. S1 C-D'). Overall, these observations suggest that the cellular arrangement of zebrafish IVDs is majorly aligned with mammalian IVDs.

ccn2a and *ccn2b* are expressed in larval notochord and adult intervertebral discs

In situ hybridization on zebrafish embryos reported that both paralogs of CCN2: *ccn2a* and *ccn2b* are expressed in notochord (Fernando et al., 2010). However, the spatiotemporal

expression pattern of *ccn2a* and *ccn2b* in notochordal tissue and IVDs remained unknown. Semi qPCR results reveal that *ccn2a* and *ccn2b* expression could be detected earliest at 9 hours post-fertilization (hpf) and 12 hpf, respectively (Fig. 1A). Whole-mount *in situ* hybridization showed that both *ccn2a*, as well as *ccn2b* transcripts are expressed in the notochord at 3 dpf (Fig. 1B). Interestingly, transverse sections of the 3 dpf whole-mount *in situ* hybridized embryos showed that *ccn2a* transcripts were localized in the NSCs, whereas *ccn2b* transcripts were detected in the NCs (Fig. 1B). *In situ* hybridization on the sagittal sections of 3 mpf zebrafish showed that both *ccn2a* and *ccn2b* were prominently expressed in the OAF and NSCs (Fig. 1C). Weak expression was visible in the IAF and NP cells (Fig. 1C). Altogether, *in situ* hybridization data suggest that *ccn2a* and *ccn2b* are heterogeneously expressed in the adult IVDs.

Next, *TgBAC*(*ccn2a*:EGFP)^{ari1} reporter line (Mukherjee et al., 2021) was employed to identify the *ccn2a* expressing cell populations. *BACccn2a*:EGFP expression mimicked endogenous *ccn2a* mRNA expression. Transverse sections of the 3 dpf embryo identified *BACccn2a*:EGFP expression in the NSCs (Fig. 1D). In line with the *in situ* analysis, in 3 mpf zebrafish, prominent *BACccn2a*:EGFP expression was seen in the OAF cells and NSCs (Fig. 1E). Weak and scattered EGFP expression was detected in IAF and NP cells (Fig. 1E). Further, immunolocalization studies detected ubiquitous CCN2 protein localization throughout the adult IVD (Fig. 1F and Fig. S2A). Further, while 24 mpf old *BACccn2a*:EGFP zebrafish IVD showed similar spatial EGFP expression like 3 mpf young adults, decreased EGFP expression was observed in 24 mpf IVD compared to their 3 mpf young siblings (Fig. S2B). In addition, the qPCR analysis showed decreased *ccn2a* transcripts in the vertebral tissues of 24 mpf animals compared to 3 mpf (Fig. S2C). Overall, *ccn2a* and *ccn2b* transcripts are expressed in the NSCs and NCs of the embryonic notochord, respectively, and in adult IVD, both paralogs are predominantly expressed in the OAF and NSCs, CCN2 protein is localized ubiquitously, and Ccn2a expression is decreased in aged IVDs.

ccn2a mutants exhibit IVDD in adult zebrafish.

Preceding results showed that *ccn2a* and *ccn2b* transcripts are expressed in the developing notochord and adult IVDs. We, therefore, sought to explore their role in IVD morphogenesis and homeostasis. To study this, we employed a loss-of-function *ccn2a* mutant allele (the *ctgfa*^{bns50} allele hereafter *ccn2a*$^{-}$) (Mokalled et al., 2016) and generated an 8 nucleotide

deletion *ccn2b* mutant allele (*ccn2b*^{ari2} allele hereafter *ccn2b*$^{-}$) (Fig. S3 A-C). qPCR analysis showed ~50% decreased *ccn2b* transcripts in 30 hpf *ccn2b*$^{-/-}$ relative to the wild-type (WT) embryos, suggesting that *ccn2b*$^{-}$ mRNA is unstable (Fig. S3D). Both *ccn2a*$^{-/-}$ and *ccn2b*$^{-/-}$ are adult viable. While *ccn2b*$^{-/-}$ morphologically remained indistinguishable from WT siblings, at least until 12 mpf (Fig. S3E), ~60% of *ccn2a*$^{-/-}$ animals showed curved-body phenotype between 10-12 mpf (Fig. 2A), which intrigued us to examine the spine structure of 12 mpf zebrafish. Alcian blue and Alizarin Red S (AB/AR) staining showed the presence of intervertebral gaps, the space occupied by the IVDs, in 12 mpf WT as well as *ccn2b*$^{-/-}$ animals (Fig. S3F); however, visible intervertebral gaps were not detected in all analyzed *ccn2a*$^{-/-}$ siblings (Fig. 2B), suggesting that IVD thinning phenotype in *ccn2a*$^{-/-}$ zebrafish is 100% penetrant.

Further, to find the onset of the IVD thinning phenotype, we explored the spine morphology from 1- to 6- mpf by AB/AR staining. *ccn2a*$^{-/-}$ showed the presence of intervertebral gaps similar to WT siblings until 4 mpf (Fig. 2C). At 6 mpf, *ccn2a*$^{-/-}$ despite being morphologically similar to WTs (Fig. S3G), a curved spine lacking visible intervertebral gaps in all investigated *ccn2a*$^{-/-}$ (Fig. 2C) indicated a possibility of IVDD. Further, µCT imaging confirmed reduced intervertebral gaps in 6 mpf *ccn2a*$^{-/-}$ compared to their WT siblings (Fig. 2D). Oegema et al. suggested that increased fibronectin expression and the fragmented appearance of the fibronectin protein in the IVD are the hallmarks of mammalian IVDD (Oegema et al., 2000). Therefore, we explored the possibility of IVDD in *ccn2a*$^{-/-}$ by analyzing the immunolocalization of fibronectin (FN1) and transcript levels of fibronectin1 paralogs; (*fn1a* and *fn1b*) in 6 mpf IVDs. Immunostaining on sagittal sections of WT zebrafish revealed that fibronectin is localized in a lamellar pattern in the IAF, with a scattered expression in the rest of the IVD (Fig. 2E). In contrast, noticeable fragmented fibronectin was detected in the IAF of age-matched *ccn2a*$^{-/-}$ IVDs (Fig. 2E). Further, fluorescence intensity analysis revealed a ~6-fold increased fibronectin expression in *ccn2a*$^{-/-}$ relative to WT (Fig. 2 E and F). Similarly, qPCR analysis showed increased *fn1a* expression in vertebral tissues of *ccn2a*$^{-/-}$ compared to WT siblings, while *fn1b* expression remained unaltered (Fig. 2G). Thus, these results suggest that deficiency of Ccn2a leads to IVD degeneration in zebrafish.

Ccn2a is necessary for OAF cell proliferation and NP cell survival in adult IVDs.

Prospective reasons for IVDD in *ccn2a*$^{-/-}$ could be inefficient cell proliferation and/or increased cell death. Since cellular homeostasis in WT zebrafish IVDs is yet to be explored, we examined cell proliferation and cell death in 4 mpf adult WT zebrafish IVDs (Fig. S4A). Interestingly, EdU incorporation data showed proliferating cells only in the OAF region (Fig. 3A). In contrast, TUNEL^{+} cells were observed in the NP region (Fig. 3B). Moreover, EdU^{+} or TUNEL^{+} cells were undetected in the IAF cells and NSCs (Fig. 3 A and B). Taken together, our study suggests that only OAF cells can proliferate while NP cells are prone to die in 4 mpf adult zebrafish IVDs.

Next, we analyzed and compared cell proliferation and cell death indices in IVDs of 4 mpf animals when intervertebral gaps were visible in *ccn2a*$^{-/-}$, similar to WT (Fig. 2B). EdU incorporation assay on sagittal vertebral tissue sections identified a ~50% reduction in OAF cell proliferation in *ccn2a*$^{-/-}$ compared to WT siblings (Fig. 3 C and D). TUNEL assay on sagittal vertebral tissue sections revealed a ~40% increased NP cell death in *ccn2a*$^{-/-}$ compared to WT siblings (Fig. 3 E and F). Further, we asked whether the cell turnover in *ccn2a*$^{-/-}$ IVDs is affected during morphogenesis. No significant difference was visible in cell proliferation as well as cell death (Fig. S4 B-F) between WT and *ccn2a*$^{-/-}$ siblings at 1 mpf, indicating normal IVD morphogenesis in *ccn2a*$^{-/-}$. Further, like 4 mpf adults, in 1 mpf juvenile animals, BrdU^{+} proliferating cells and TUNEL^{+} cells were found only in the OAF and NP regions, respectively (Fig. S4 C and E). Altogether, these observations suggest that though *ccn2a*$^{-/-}$ appears to develop normal IVDs, Ccn2a is required for OAF cell proliferation and NP cell survival in adult zebrafish IVDs.

Ccn2a regulates *shha* and *shhb* expression in adult IVDs.

In mammals, several growth factors and collagens are associated with IVDD. Increased TGFβ1 (Peng et al., 2009) and BMP2 (Hollenberg et al., 2021) expression were observed in degenerating human IVDs. It is also reported that Shh positively regulates NP cell proliferation in embryonic and postnatal mouse IVDs (Choi and Harfe, 2011; Dahia et al., 2012), and its expression decreases with age progression (Winkler et al., 2014) Besides the growth factors, collagens are also associated with IVD maintenance in mammals (Trefilova et al., 2021). Since adult *ccn2a*$^{-/-}$ showed disc degeneration, we intended to analyze expression levels of growth factor and collagen coding genes in 4 mpf zebrafish vertebral tissues. qPCR analysis revealed a reduction in transcript levels of *shha* (~36%) and *shhb* (~44%), while

those of other analyzed growth factor and collagen coding genes remained indistinguishable (Fig. 3G) in vertebral tissues of *ccn2a*$^{-/-}$ compared to WT.

Next, *in situ* hybridization analysis detected ubiquitous *shha* and *shhb* expression in the WT IVDs (Fig. 3H). Notably, consistent with the qPCR data, reduced expression of *shha* and *shhb* was detected in the *ccn2a*$^{-/-}$ IVDs without altering the spatial expression pattern (Fig. 3H). Moreover, immunohistochemistry found ubiquitous localization of Shha in WT IVDs with a ~60% decreased expression in *ccn2a*$^{-/-}$ IVDs compared to WT (Fig. S5 A and B). Decreased expression of *shha* and *shhb* transcripts, as well as Shha protein intrigued us to explore whether SHH signaling is affected in *ccn2a*$^{-/-}$. qPCR analysis showed decreased expression of SHH target genes *gli1*, *ptch1*, and *ptch2* (Bonifas et al., 2001; Chuang et al., 2003; Litingtung et al., 1998) in vertebral tissues of *ccn2a*$^{-/-}$ compared to WT (Fig. 3I). Overall, Ccn2a positively regulates SHH signaling by modulating *shha* and *shhb* expression in adult zebrafish IVDs.

FGFR1 signaling induces *shha* and *shhb* expression and cellular homeostasis in adult IVDs.

Next, we intended to explore the underlying signaling cascade in Ccn2a mediated regulation on *shha* and *shhb* expression in adult IVDs. Studies suggest that *Shh* is a downstream target of Fgfr1 and Fgfr2 during limb (Verheyden et al., 2005) and heart (Lavine, 2006) morphogenesis. Dahia et al. have shown that pan FGFR signaling is active in the AF region but not in the NP region of the postnatal and adult mouse IVDs (Dahia et al., 2009). Moreover, FGFR1 (Li et al., 2008; Yan et al., 2015) and FGFR3 (Yan et al., 2015) are expressed differentially in degenerated human discs. Our preceding results showed that IVDD is initiated at 4 mpf in *ccn2a*$^{-/-}$. Therefore, a comparative qPCR was performed to identify whether FGF receptor coding genes are differentially expressed in 4 mpf *ccn2a*$^{-/-}$ vertebral tissues. Our assessment revealed a ~2-fold increased expression of *fgfr1b*, a zebrafish paralog of human *FGFR1*, in vertebral tissues of *ccn2a*$^{-/-}$ compared to WT, while expression of *fgfr1a*, another paralog of human *FGFR1*, and other FGFRs remained unaffected (Fig. 4A). Further, *in situ* hybridization showed ubiquitous *fgfr1a* and *fgfr1b* expression in WT IVDs (Fig. 4B). Consistent with qPCR data, *fgfr1b* transcripts were predominantly induced in the *ccn2a*$^{-/-}$ IVDs compared to WT, while *fgfr1a* expression remained unaffected (Fig. 4B). Altered *fgfr1b* expression in *ccn2a*$^{-/-}$ IVDs, indicates that Fgfr1b signaling could be involved with the IVD degeneration. Further, published evidence

and altered expression of *shha*, *shhb*, and *fgfr1b* led us to hypothesize that FGFR1 signaling is associated with the *shha* and *shhb* expression in adult zebrafish IVDs. To investigate this, we used pharmacological and genetic approaches. In the pharmacological approach, we inhibited the FGFR1 signaling for 4 days in 4 mpf WT zebrafish by intraperitoneal injection of PD166866, an FGFR1 specific inhibitor (Fig. 4C) (Panek et al., 1998). To identify whether PD166866 inhibits FGFR1 signaling in the zebrafish vertebral tissues, we explored the expression of zebrafish orthologs of FGFR1 signaling target genes CCND1, CCND2 (Koziczak et al., 2004) ETV4, and ETV5 (DeSalvo et al., 2021) expression upon PD166866 treatment. qPCR analysis of the vertebral tissues showed decreased *ccnd1*, *ccnd2a*, *ccnd2b*, *etv4*, and *etv5a* gene expression in the PD166866 treated animals compared to the control (Fig. S6A), indicating PD166866 inhibits FGFR1 signaling in zebrafish vertebral tissues. Further, qPCR analysis showed a ~40% decreased expression of *shha* and *shhb* (Fig. 4D), while transcript levels of *fgfr1b* and *ccn2a* remained unaffected upon PD166866 treatment (Fig. 4E), indicating that FGFR1 signaling induces *shha* and *shhb* expression, but not *ccn2a*, in adult IVDs.

To further confirm, we examined the transcript levels of *shha* and *shhb* in vertebral tissues of *ccn2a*$^{-/-}$ upon ectopic activation of FGFR1 signaling. We carried out FGFR1 gain-of-function experiments using *Tg(hsp70:ca-fgfr1)* zebrafish, which ubiquitously expresses a constitutively active form of *Xenopus* Fgfr1 upon heat shock (Marques et al., 2008). We raised *ccn2a*$^{-/-}$ on *hsp70:ca-fgfr1* background (hereafter *ccn2a*$^{-/-,fgfr1\text{-}ca}$). WT, *ccn2a*$^{-/-}$, and *ccn2a*$^{-/-,fgfr1\text{-}ca}$ siblings were subjected to heat shock from 2.5- to 4 mpf, and RNA was extracted from vertebral tissues 24 h post last heat shock (Fig. 4F). Consistent with the pharmacological inhibition data, qPCR analysis revealed a ~2-fold increased expression of FGFR1 downstream target genes *ccnd1*, *ccnd2a*, *ccnd2b*, *etv4*, and *etv5a* expression (Fig. S6B) and a ~2.5-fold increased *shha* and *shhb* expression upon ectopic expression of the constitutively active form of *Xenopus* Fgfr1 in *ccn2a* mutants, while *fgfr1b* expression remained unaltered (Fig. 4G). Thus, pharmacological inhibition and gain-of-function studies revealed that FGFR1 signaling induces *shha* and *shhb* expression in vertebral tissues. Overall, data suggest that *shha* and *shhb* are common downstream targets of Ccn2a and FGFR1 signaling. Notably, in *ccn2a*$^{-/-}$ IVDs, despite the increased *fgfr1b* expression (Fig. 4 A and B), decreased FGFR1 target gene *shha* and *shhb* expression (Fig. 3 G and H) was observed, which could be rescued by ectopic expression of the active form of Fgfr1 (Fig. 4G) indicating that Ccn2a is required for FGFR1 activation in adult IVDs.

As *ccn2a*$^{-/-}$ IVDs showed altered cellular homeostasis, and Ccn2a, as well as FGFR1 signaling, induce *shha* and *shhb* expression, we analyzed the cell proliferation and cell survival in adult IVDs upon inhibition of FGFR1 signaling. EdU incorporation and TUNEL assay revealed that 4 days of PD166866 treatment (Fig. 4H) resulted in decreased OAF cell proliferation (Fig. 4 I and J) and increased NP cell death (Fig. 4 K and L), similar to the phenotype observed in the adult *ccn2a*$^{-/-}$ IVDs. Taken together, these observations indicate that, similar to Ccn2a, FGFR1 signaling induces *shha* and *shhb* expression, OAF cell proliferation, and NP cell survival in adult IVDs.

Ectopic activation of Fgfr1 signaling restores intervertebral disc in adult *ccn2a*$^{-/-}$.
As our data showed that Ccn2a, as well as FGFR1 signaling, induce OAF cell proliferation and NP cell survival and Ccn2a is not a downstream target of FGFR1 signaling, we were curious to investigate whether ectopic expression of a constitutively active form of *Xenopus* Fgfr1 can reinstate the cellular phenotype of *ccn2a*$^{-/-}$ IVDs. To address this, WT, *ccn2a*$^{-/-}$, and *ccn2a*$^{-/-,fgfr1\text{-}ca}$ siblings were subjected to heat shock from 2.5- to 4 mpf, followed by EdU incorporation and TUNEL assay (Fig. 5A). Analysis revealed a ~95% increase in OAF cell proliferation (Fig. 5 B and C) and a ~75% decrease in NP cell death (Fig. 5 D and E) in *ccn2a*$^{-/-,fgfr1\text{-}ca}$ compared to *ccn2a*$^{-/-}$. Notably, OAF cell proliferation and NP cell death in *ccn2a*$^{-/-,fgfr1\text{-}ca}$ were comparable with the WT IVDs (Fig. 5 B-E). Moreover, extended ectopic activation of FGFR1 signaling from 2.5- to 6 mpf could maintain the intervertebral gaps in *ccn2a*$^{-/-}$ (Fig. 5 F and G), suggesting ectopic activation of FGFR1 signaling can restore IVDs by augmenting OAF cell proliferation and NP cell survival in *ccn2a*$^{-/-}$.

SHH signaling regulates OAF cell proliferation and NP cell survival in adult IVDs.
Next, we explored whether Ccn2a or FGFR1 signaling-mediated OAF cell proliferation and NP cell survival are regulated through the SHH pathway. To test this, cyclopamine, an SHH signaling inhibitor (Incardona et al., 1998) was injected to 4 mpf WT zebrafish for 4 days (Fig. S7A), followed by gene expression, cell death, and cell proliferation analysis were performed. qPCR analysis of vertebral tissues revealed decreased SHH target gene *gli1*, *ptch1*, and *ptch2* expression without affecting *shha* and *shhb* transcripts in cyclopamine injected compared to DMSO injected siblings indicating SHH signaling inhibition (Fig. S7B). Moreover, SHH signaling inhibition leads to suppression of OAF cell proliferation (Fig. 5 H and I) and increased NP cell death (Fig. 5 J and K), indicating the positive role of SHH signaling in OAF cell proliferation and NP cell survival in adult IVDs. Overall, these results

indicate that, presumably, Ccn2a and FGFR1 signaling induce OAF cell proliferation and NP cell survival through the SHH pathway in adult IVDs.

Ccn2a induces regenerative processes in aged IVDs through FGFR1 signaling.

Micro-CT analysis showed signs of disc degeneration in 12 mpf WT zebrafish (Kague et al., 2021). Hence, we compared the *shha* and *shhb* expression, OAF cell proliferation, and NP cell death in 4- and 12 mpf WT vertebral tissues. We found decreased *shha* and *shhb* expression (Fig. 6A), reduced OAF cell proliferation (Fig. 6 B and C), and increased NP cell death (Fig. 6 D and E) in 12 mpf compared to 4 mpf WT IVDs. Interestingly, similar to juvenile and 4 mpf adults, in 12 mpf-aged animals, EdU^{+} proliferating cells and $TUNEL^{+}$ cells were found only in the OAF and NP regions, respectively (Fig. 6 B and D). Overall, the observed cellular phenotype and genetic regulation in 12 mpf IVDs were similar to 4 mpf *ccn2a*$^{-/-}$ IVDs, and decreased *ccn2a* expression was observed in aged IVDs. Hence, we sought to assess the potency of Ccn2a to promote regeneration in aged IVDs. We used *hsp70:ctgfa-FL-2a-EGFP* (henceforth *ccn2a*$^{+/+,hsp70:ctgfa}$) transgenic zebrafish (Mokalled et al., 2016), which ubiquitously expresses Ccn2a upon heat shock. Heat shock treatments for 7 days (Fig. 6F) resulted in a ~4-fold increase in *ccn2a* expression along with increased *shha* and *shhb* expression in vertebral tissues of 12 mpf *ccn2a*$^{+/+,hsp70:ctgfa}$ relative to *ccn2a*$^{+/+}$ siblings (Fig. 6G). Moreover, EdU incorporation and TUNEL assay (Fig. 6F) showed that ectopic Ccn2a expression resulting induction in OAF cell proliferation (Fig. 6 H and I) and NP cell survival (Fig. 6 J and K), suggesting that in aged vertebral tissues, Ccn2a induces *shha* and *shhb* expression and can promote cellular processes involved in IVD regeneration. Our study identified that Ccn2a and FGFR1 signaling induce *shha* and *shhb* expression, NP cell survival, and OAF cell proliferation in adult IVDs, and Ccn2a is not a downstream target of FGFR1 signaling. Thus, we intended to explore whether Ccn2a exerts its regulation through the FGFR1 signaling cascade in adult IVDs. We combined genetic and pharmacological approaches on 12 mpf animals to dissect this. Control groups (*ccn2a*$^{+/+}$ and *ccn2a*$^{+/+,hsp70:ctgfa}$) received DMSO, while test group (*ccn2a*$^{+/+,hsp70:ctgfa}$) received PD166866 injection from day- 4 to 6, all groups received heat shock from day- 0 to 6, and animals were sacrificed on day 7 (Fig. 6L). Animals used for cell proliferation assay received a single EdU injection on day 6 (Fig. 6L). qPCR analysis revealed an increased expression of *shha* and *shhb* (Fig. 6M) as well as FGFR1 downstream target genes *ccnd1*, *ccnd2a*, *ccnd2b*, *etv4*, and *etv5a* expression (Fig. S8A) in the vertebral tissues upon overexpression of Ccn2a. Further, PD166866 treatment suppressed the ectopic Ccn2a mediated induction on *shha* and *shhb*

(Fig. 6M) and FGFR1 signaling target genes (Fig. S8B) expression without affecting *ccn2a* expression (Fig. 6M), indicating that, Ccn2a induces *shha* and *shhb* expression through FGFR1 signaling.

Next, to confirm the link between Ccn2a and FGFR1 signaling, we used SU5402, another FGFR1 signaling inhibitor (Mohammadi et al., 1997) (Fig. S8C). Gene expression analysis showed decreased FGFR1 target genes *ccnd1*, *ccnd2a*, *ccnd2b*, *etv4*, and *etv5a* expression (Fig. S8D), indicating SU5402 inhibits FGFR1 signaling in zebrafish vertebral tissues. Moreover, in the SU5402 treated animals, decreased *shha* and *shhb* expression was observed, while *fgfr1b* and *ccn2a* remained unaffected (Fig. S8E). Next, we performed the pharmacological inhibition in combination with the genetic overexpression of Ccn2a (Fig. S8F). In line with PD166866 inhibition, SU5402 treatment suppressed the ectopic Ccn2a-mediated increased FGFR1 downstream target genes (Fig. S8G) as well as *shha* and *shhb* expression without affecting the *ccn2a* expression (Fig. S8H). Overall data confirms that Ccn2a induces *shha* and *shhb* expression through FGFR1 signaling.

Further, in Ccn2a overexpression animals, ectopic Ccn2a mediated increased OAF cell proliferation, and NP cell survival was suppressed upon PD166866 treatment (Fig. 6 N-Q). As short-term ectopic Ccn2a showed induction on OAF cell proliferation and NP cell survival in aged IVDs, we intended to explore the effect of the ectopic Ccn2a expression for an extended period on degenerated IVD. Thus, 12 mpf old no background (control) and *hsp70*:*ctgfa* animals were given daily 1 h heat shock for 90 days (Fig. 6R). Skeletal staining of the animals post-90 days of treatment showed visibly increased intervertebral gaps in Ccn2a-overexpressing animals compared to their no-background siblings (Fig. 6S). Altogether, in degenerated IVDs, Ccn2a induces regeneration by inducing *shha* and *shhb* expression, OAF cell proliferation, and NP cell survival through FGFR1 signaling.

Ccn2a interacts with the C-terminal fragment of Fgfr1a and Fgfr1b.

Preceding results revealed that Ccn2a plays a central role in the maintenance and regeneration of IVDs through FGFR1-SHH signaling in adult zebrafish. Hence, we explored the molecular cross-talk between Ccn2a and zebrafish orthologs of FGFR1 viz. Fgfr1a and Fgfr1b by proximity ligation assay (PLA). *In vitro* synthesized C-terminal Myc-tagged full-length *ccn2a* (Ccn2a-FL^{Myc}) mRNA was co-injected with C-terminal FLAG-tagged- *fgfr1a* (Fgfr1a^{FLAG}) or *fgfr1b* (Fgfr1b^{FLAG}) mRNA into one-cell stage zebrafish egg (Fig. 7A).

Immunostaining against Myc and FLAG on injected embryos confirmed tagged Ccn2a-FL, Fgfr1a, and Fgfr1b expression (Fig. S9 A and B). PLA on 30 hpf embryos showed that zebrafish Ccn2a-FL interacts with Fgfr1a as well as Fgfr1b (Fig. 7 B and C).

Ccn2a is a modular protein with four interaction domains and a hinge region at which it cleaves into a pro-fibrotic N-terminal fragment (NTF) and a proliferative C-terminal fragment (CTF) (Fig. S9C) (Grotendorst and Duncan, 2005; Robinson et al., 2012), and our PLA showed the interaction between C-terminal tagged Ccn2a-FL and Fgfr1a, or Fgfr1b (Fig. 7 B and C) indicating that the CTF of Ccn2a interacts with Fgfr1a or Fgfr1b. To further explore whether the NTF of Ccn2a interacts with the Fgfr1a and Fgfr1b, *in vitro* synthesized mRNA of C-terminal Myc-tagged IGFBP and vWC domain coding NTF of *ccn2a* (Ccn2a-NTF^{Myc}) was co-injected with Fgfr1a^{FLAG} or Fgfr1b^{FLAG} mRNA (Fig. 7A). Immunostaining against Myc and FLAG on injected embryos confirmed tagged Ccn2a-NTF, Fgfr1a, and Fgfr1b expression (Fig. S9 D and E). PLA analysis on 30 hpf embryos indicated that the NTF of Ccn2a does not interact with Fgfr1a (Fig. S9F) or Fgfr1b (Fig. S9G). Overall, C-terminal tagged full-length Ccn2a but not the C-terminal tagged NTF of Ccn2a interacts with Fgfr1a and Fgfr1b, indicating Ccn2a interacts with the ligand-receptor complex of Fgfr1a as well as Fgfr1b through its C-terminal fragment.

Discussion

This study provides novel insights into the mechanism by which Ccn2a maintains the IVD's tissue integrity and its potential role in regeneration in degenerated aged IVD. *ccn2a* is expressed by the OAF cells, and NSCs and Ccn2 protein is localized ubiquitously in adult IVDs. Mechanistically, Ccn2a promotes OAF cell proliferation and NP cell survival by inducing FGFR1-SHH signaling in young as well as aged adult IVDs. Based on the above findings, we propose that Ccn2a is an essential component of IVD homeostasis and can induce IVD regeneration.

In agreement with notochord-specific Ccn2 knockout mice (Bedore et al., 2013) data, we found that global loss of Ccn2a in zebrafish leads to an early IVDD. It is interesting to note that *Ccn2* global knockout mice die after birth (Ivkovic et al., 2003); however, *ccn2a*$^{-/-}$ zebrafish survive adults. Unlike mammals, zebrafish have two paralogs of *CCN2*: *ccn2a* and *ccn2b*, and both are expressed in larval notochord. qPCR analysis identified ~4-fold

increased expression of *ccn2b* in *ccn2a*$^{-/-}$ larvae compared to WT (Fig. S10), indicating that possibly in the absence of Ccn2a, increased Ccn2b contributes to the normal development of the *ccn2a*$^{-/-}$.

Our cell proliferation and cell death analysis in the juveniles, 4 mpf young adults, as well as 12 mpf aged animals, found that zebrafish IVDs carry distinct cell proliferation and cell death regions. Like mammals (Dahia et al., 2009), NP cells of adult zebrafish IVDs are prone to die; however, unlike mammals, they are not proliferating. In zebrafish embryos, upon injury, dead notochordal cells get replenished by the cells derived from NSCs (Garcia et al., 2017). Since, in adult IVDs, only the OAF cells are proliferating (Fig. 3A), presumably subpopulation of OAF cells migrates, differentiates, and replenishes different cell populations in IVDs. Further, studies in rabbits and humans have shown the presence of stem cells in the cartilaginous endplates that proliferate and differentiate into different cell types of IVDs (Henriksson et al., 2009). Thus, it will be interesting to know whether, like mammals, zebrafish IVDs have an external source of cells to replenish the dead cells or the proliferating OAF cells have multipotent characters, and these are the sole source of all types of cells in zebrafish IVDs.

In adult IVDs, FGFR1 signaling induces *shha* and *shhb* expression (Fig. 4G). Surprisingly, in *ccn2a*$^{-/-}$ IVDs, despite increased *fgfr1b* transcripts (Fig. 4 A and B), its downstream targets are downregulated (Fig. 3 G and H). Thus, it is possible that since Ccn2a induces FGFR1 signaling, in *ccn2a*$^{-/-}$, decreased levels of Shha and Shhb induce *fgfr1b* expression via a feedback loop mechanism. However, changes in the *shha* and *shhb* transcripts levels upon pharmacological inhibition of FGFR1 signaling in WT animals (Fig. 4D) or ectopic expression of a constitutively active form of Fgfr1 in *ccn2a*$^{-/-}$ (Fig. 4G) did not affect the transcript levels of *fgfr1b* (Fig. 4 E and G), ruling out the presence of feedback loop between the *fgfr1b* and its downstream molecules in adult vertebral tissues. Further, *in vivo* PLA showed that Ccn2a binds to Fgfr1a as well as Fgfr1b, suggesting Ccn2a can signal through both the paralogs and is an integral part of the FGFR1 ligand-receptor complex for the receptor activation. Notably, altered expression of *fgfr1b* in *ccn2a*$^{-/-}$ indicates that presumably, Ccn2a signals through the Fgfr1b as its preferred receptor. The absence of a feedback loop between the Fgfr1b and its downstream targets and upregulation of *fgfr1b* in the *ccn2a*$^{-/-}$ IVDs indicates that plausibly, Ccn2a dependent active form of Fgfr1b ligand-

receptor complex regulates *fgfr1b* expression through an unknown mechanism; which needs to be elucidated.

It is believed that in IVDs, CCN2 is a pro-fibrotic molecule, as in degenerated human discs, *CCN2* is up-regulated (Peng et al., 2009). In contrast, our study on zebrafish found that overexpression of Ccn2a induces regenerative cellular processes in degenerated IVDs. PLA showed that only CTF, which is known to be a pro-proliferative fragment (Grotendorst and Duncan, 2005; Robinson et al., 2012), interacts with Fgfr1a as well as Fgfr1b, supporting that Ccn2a is pro-regenerative rather than a pro-fibrotic molecule in IVDs. It could be possible that in aged human IVDs, CCN2 induction is a regenerative response; however, the amount of CCN2 is insufficient to induce effective regeneration in degenerated discs. In the future, it will be interesting to explore whether an external supply of a higher amount of CCN2 can induce regeneration in degenerated mammalian IVDs. Further, Ccn2a promotes IVD regeneration via inducing FGFR1 signaling in zebrafish IVDs (Fig. 6). Thus, comparative studies exploring the effect of FGFR1 agonists or CCN2 on mammalian IVD regeneration may open new avenues to develop therapeutic strategies to manage IVD regeneration in humans.

In conclusion, our study shows that Ccn2a is a crucial secreted molecule in IVD maintenance. Moreover, induction of cell proliferation and suppression of cell death by ectopic Ccn2a in degenerated IVDs shows its potential to induce IVD regeneration. This study increases our understanding of the cellular homeostasis of the zebrafish IVDs, and the essential role of Ccn2a-FGFR1-SHH signaling in IVD maintenance and regeneration, which provides potential therapeutic implications of CCN2 to promote regeneration in degenerated human discs.

Materials and Methods

Ethics statement

Zebrafish care procedures and protocols used in this study were as per guidelines of the Committee for the Purpose of Control and Supervision of Experiments on Animals (CPCSEA), Government of India, and approved by The Institute Animal Ethics Committee (IAEC).

Zebrafish maintenance

Zebrafish were maintained in a state-of-the-art zebrafish aquarium as previously described (Aleström et al., 2020). Animals ranging from fertilized eggs to 24 mpf were used in this study. The genotype of animals used is specified in Fig. and figure legends. Clutch mate adult male fish of similar size were used for the experiments associated with PD166866 or cyclopamine treatment. For the rest of the experiments, clutch mate control and test fish of similar size and equal sex distribution were used for each age group.

Generation of *ccn2b* mutant (*ccn2b*^{ari2}) zebrafish

TALEN was used to generate the *ccn2b*^{ari2} mutant allele. TALEN constructs for left and right arms were designed to target exon 2, with 17-19 bp long repeat-variable di-residue (RVD) binding sequence and a 15 bp long spacer; left arm sequence: TGATTGCCCAGACGAGA; right arm sequence: TAGGCACCAGTCTAGTGTT. Left and right arm TALEN pair constructs were generated with the help of the Golden Gate TALEN assembly strategy (Cermak et al., 2015). TALEN mRNAs were synthesized using an in vitro mMESSAGE mMACHINE™ kit, following manufacturer instructions. 200 pg mRNA of each arm was injected into one-cell stage eggs to generate mutants. Injected eggs were raised and screened for germline transmission. Indel detection at the target locus was performed by High-Resolution Melting Curve Analysis (HRMA) of the gDNA isolated from caudal fins of adult F1 animals. Indels were analyzed by sequencing the PCR amplified product using a primer pair; forward, CTGCTCTCAGCCCTGTGATT; reverse, CAGCAGCTACAGCCGTCTAA, binding to the flanking region of the TALEN target. The *ari2* allele (referred to as *ccn2b*$^{-}$), harboring an 8-nt deletion, was selected and used in this study. For genotyping and gene expression analysis by qPCR forward, TGATTGCCCAGACGAGAGCCC; and reverse, CAGCAGCTACAGCCGTCTAA, primer pair was used. qPCR was performed to check *ccn2b*$^{-}$ transcript stability. Transcript levels of *ccn2b*$^{-}$ in *ccn2b*$^{-/-}$ were quantitated relative to the average expression level *ccn2b*$^{+}$ in wild-type controls and were normalized to *ef1α* expression levels.

qPCR and gene expression analysis

According to the manufacturer's instructions, total RNA from embryos and adult vertebral tissues was extracted using TRIzol® reagent (Invitrogen). Total RNA was isolated from 30 pooled embryos/ biological replicates for embryonic stages. For adult vertebral tissues, animals were sacrificed, and vertebral tissues were isolated manually by removing the

head, organs, fins, skin, skeletal muscles, and spinal cord as much as possible without disturbing the vertebral column and processed for total RNA isolation. Further, 1-4 µg of total RNA was reverse transcribed into cDNA using MMLV reverse transcriptase (Invitrogen- 28025013). The prepared cDNA was used to perform qPCR in a PCR Max Real-time PCR detection system (Cole Parmer) using iTaq™ Universal SYBR® Green Supermix (Bio-Rad- 1725124) and gene-specific prime pair (Table S1). Transcript levels of genes analyzed in test samples were quantitated relative to the control samples' average expression level and normalized to *ef1α*. All reactions were run in triplicate. Gene expression fold changes were calculated using the ΔCt method. For adults, each sample represents one animal.

Molecular cloning

For making riboprobes against zebrafish *ccn2b, fgfr1a, fgfr1b, shha, and shhb mRNA, partial cDNA* was amplified from embryonic cDNA using gene-specific primers (Table S2) and cloned into the pGEM®-T Easy vector (Promega) to create pGEMTeasy-Z*ccn2b,* pGEMTeasy-Z*fgfr1a,* pGEMTeasy-Z*fgfr1b,* pGEMTeasy-Z*shha, and* pGEMTeasy-Z*shhb constructs.*

For proximity ligation assay (PLA), coding sequences of full-length zebrafish *ccn2a*, N-terminal fragment of *ccn2a*, full-length *fgfr1a,* and full-length *fgfr1b* were amplified from embryonic cDNA using gene-specific primers (Table S3). Full-length *ccn2a* and N-terminal fragment of *ccn2a* (aa 1-162) were cloned into the pCMV-Myc-C vector (Clontech), while full-length *fgfr1a* and *fgfr1b* were cloned into the p3xFLAG-CMV-14 vector (Merck). Full-length *ccn2a*, N-terminal fragment of *ccn2a*, full-length *fgfr1a*, and full-length *fgfr1b* along with C- terminal MYC or FLAG tag were amplified from respective constructs using specific primers and subcloned into the pCS2+ vector to create FL-Z*ccn2a*-MYC, NTF-Z*ccn2a*-MYC, FL-Z*fgfr1a*-FLAG, and FL-Z*fgfr1b*-FLAG (Table S3), respectively, for the synthesis of *in vitro* capped mRNA.

***In situ* hybridization**

Digoxigenin (DIG) labeled *ribo*probes against *ccn2a, ccn2b, fgfr1a, fgfr1b, shha, and shhb* were synthesized using linearized pGEMTeasy-Z*ccn2b,* pGEMTeasy-Z*fgfr1a,* pGEMTeasy-Z*fgfr1b,* pGEMTeasy-Z*shha, and* pGEMTeasy-Z*shhb constructs, respectively,* and T7 RNA polymerase (Roche- 10881767001).

For whole-mount in situ hybridization (WISH), from around 24 hpf, embryos were treated with 0.2 mM 1-phenyl-2-thiourea to prevent pigmentation, and embryos were fixed in 4% paraformaldehyde, washed twice with 0.2 % Tween-20 in 1X PBS, dehydrated, and processed for WISH utilizing digoxigenin-labeled riboprobes against, *ccn2a* (Mukherjee et al., 2021), and *ccn2b*. For sectioning after signal development, embryos were washed with deionized water, fixed in 4% paraformaldehyde, dehydrated in 30% sucrose, and embedded in the tissue freezing medium (Leica- 14020108926). 10µm thin transverse sections through the trunk were cut (Leica CM1520), air dried, washed in PBS, mounted in the Kaiser's gelatin glycerol (Merck), and imaged with an Olympus BX53 bright-field microscope.

For in situ hybridization on sections, fixed tissues were processed for wax sectioning, and *in situ* hybridization was performed as described previously (Lepilina et al., 2006). 12µm thin sagittal sections through the trunk were mounted on a charged glass slide (Thermo Fisher Scientific), rehydrated, permeabilized with proteinase K at 37°C, acid washed, and hybridized with DIG-labelled riboprobes (1 µg/mL in hybridization buffer) at 65°C overnight. On the second day, sections were briefly washed with wash buffer, blocked in blocking buffer, and incubated overnight with an alkaline phosphatase-conjugated anti-DIG antibody (Roche- 11093274910) at 4°C. On the third day, sections were washed, and the signal was detected with BM Purple staining solution (Roche- 11442074001). Further, sections were dehydrated through ethanol grades, xylol, and xylene and mounted in Entellan (Merck) for imaging.

Skeletal staining

Skeletal staining was performed as previously described (Kessel and Gruss, 1991). Briefly, fish were sacrificed at desired time points, deskinned, and fixed in 96% ethanol for 24 h and subsequently in acetone for 48 h. Fixed samples were incubated in the Alcian blue 8GX (Merck) and Alizarin Red S (Merck) staining solution for 6 h and 2 h, respectively, at 37°C. Stained samples were placed under tap water to wash off the excess stain and cleared in 1% KOH overnight at RT. The following day, samples were cleared in grades of glycerol (50% and 70%) in 1% KOH and then 100% glycerol. Lateral views of the zebrafish spines of the cleared samples were imaged with a stereoscope (Leica M205FA) or a digital single-lens reflex camera (Canon 600D).

Micro-computed tomography

6 mpf wild-type and *ccn2a*$^{-/-}$ fish were anesthetized in 0.02% tricaine in the system water. The caudal part of the wild-type and *ccn2a*$^{-/-}$ vertebral column were scanned using a SkyScan 1276 micro-CT scanner (Bruker, Germany) voxels sized 10 µm. Detailed geometric analysis was performed using an X-ray source of 200 kV, 60 µA with an Al 0.5 mm filter. Images were reconstructed using NRecon Reconstruction Software (Micro Photonics Inc.).

Heat-shock treatment

For heat-shock experiments, *Tg(hsp70l:Xla. Fgfr1,cryaa:DsRed)*^{pd3} raised in ccn2a$^{-/-}$ background, and *Tg(hsp70:ctgfa-FL-2a-EGFP)* raised in WT background were used. These transgenic animals and their respective controls received heat shock by incubation in preheated system water at 37°C for 1 h (maximum 6 fish per liter water) in 24 h intervals for the desired period. The age and genotype of animals are mentioned in each figure. Animals were sacrificed 24 h after the last heat shock and processed for qPCR, histological analysis, and skeletal staining.

Tissue sectioning

At desired time points, fish were sacrificed, cut in two halves at the anal fin, and the caudal part of each fish was fixed in 4% PFA overnight at RT. Fixed caudal parts were washed with PBS several times, deskinned, and decalcified in 0.5M EDTA (pH 8.0) in PBS for 4 days at RT. For wax sectioning, tissues were washed with PBS and dehydrated with a series of ethanol grades (50%, 70%, 90%, 100%) prior to embedding in wax, and 10µm thin tissue sections were cut with a microtome (Bright Instruments/ Leica Histocore Autocut). For cryosectioning, fixed tissues were washed with PBS, dehydrated in 30% sucrose in PBS, embedded in tissue freezing medium (Leica- 14020108926), and 10µm thin tissue sections were cut with a cryomicrotome (Leica CM1520).

Cell proliferation assay

For EdU incorporation analysis, fish were anesthetized with 0.02% tricaine in system water, and 10 µl of 10 mM EdU was injected intraperitoneally. Fish were sacrificed 24 h post-EdU injection, fixed in 4% PFA overnight at RT, decalcified in 0.5M EDTA (pH 8.0) in PBS for 4 days at RT, and cryosectioned prior to EdU labeling. EdU labeling was performed on the 10 µm thin sagittal tissue sections through the vertebral column using Click-iT^{TM} EdU Cell Proliferation Kit (Thermo Fisher Scientific- C10340) according to the

manufacturer's instructions, and DAPI (1 µg/mL in PBS) was used to stain nuclei. For imaging, sections were mounted in Mowiol® 4-88 Reagent (Merck).

For BrdU incorporation analysis, 1 mpf animals were treated with BrdU (100 µg/ml) in system water for 2 days before fixing in 4% PFA overnight at RT. Fixed animals were processed for cryosectioning. For BrdU detection, tissue sections were air-dried and washed in PBS, refixed in 4% PFA, and treated with 1N HCl in PBS at 37°C for 1h. Later, sections were blocked in blocking solution (5% goat serum (MP Biomedicals)/0.5% Triton X-100/ PBS) for 1 h and incubated with BrdU antibody (1:200) (Abcam- Ab6326) overnight at 4°C. Primary immune complexes were detected using goat, anti-rat Alexa Flour™ 488-conjugated secondary antibodies (1:400) (Thermo Fisher Scientific- A11006), and DAPI (1 µg/mL PBS) was used to detect nuclei. For imaging, stained sections were mounted in Mowiol® 4-88 Reagent (Merck- 475904). Six animals from test and control groups, from two independent experiments, were used to quantify OAF cell proliferation indices. At least 2 IVDs from each animal and 4 sections from each IVD were analyzed for quantification.

Cell death assay

Fluorescence Terminal deoxynucleotidyl transferase dUTP Nick-End Labeling (TUNEL) assay was performed to detect dead cells in the IVDs. For fluorescence TUNEL assay, 10µm thin sagittal cryosections of the caudal part of the desired genotype and aged zebrafish were prepared as described under "Tissue sectioning." TUNEL assay was performed on the cryosections using a Click-iT™ TUNEL Alexa Fluor™ 647 Imaging kit (Thermo Fisher Scientific- C10247) following the manufacturer's instructions. DAPI (1 µg/mL PBS) was used to detect nuclei. For imaging, sections were mounted in Mowiol® 4-88 Reagent (Merck), and images were acquired with a Leica SP8 confocal microscope (Leica Microsystems, Germany). Six animals from test and control groups from two independent experiments were used to quantify NP cell death indices. At least 2 IVDs from each animal and 4 sections from each IVD were analyzed for quantification.

Immunolocalization studies

Immunolocalization studies were performed on the tissue sections, as described previously (Patra et al., 2017). Briefly, PBS-washed tissue cryosections were refixed, permeabilized with 0.5% Triton X-100, blocked for 1 h in a blocking solution (5% goat serum (MP Biomedicals)/0.5% Triton X-100/ PBS), and incubated with primary antibodies against

CTGF (1:100) (Abcam- Ab6992) or Shha (1:100) (Anaspec- S-55574) or Fibronectin (1:600) (Merck- F-0635) overnight at 4°C. The goat, anti-rabbit Alexa Flour™ 647-conjugated secondary antibody (1:400) (Thermo Fisher Scientific- A32733) detected primary immune complexes. DAPI (1 µg/mL PBS) was used to detect nuclei. Sections were mounted in Mowiol® 4-88 Reagent (Merck) before imaging with a Leica SP8 laser scanning microscope (Leica Microsystems, Germany).

Wheat germ agglutinin (WGA) staining labeled the cell membrane. For WGA labeling, cryosections through the vertebral tissues were incubated in Alexa Flour™ 633 conjugated WGA (2 µg/mL in PBS) (Biotium-29024) for 1 h at room temperature before permeabilization. Sections were stained with DAPI to label nuclei before embedding in the mounting medium (Mowiol® 4-88, Merck). Images were captured on a Leica SP8 laser scanning microscope, and images were processed and analyzed with LAS X (Leica Microsystems, Germany). At least 2 IVDs from each animal and 4 sections from each IVD were analyzed for quantification.

Drug treatment

Fish were anesthetized in 0.02% Tricaine in system water for body weight determination and intraperitoneal injection. For body weight determination, anesthetized fish were kept on tissue paper to remove water from the body surface and weigh the fish. The drug dose for individual fish was calculated based on the body weight. The next day intraperitoneal injections of the drugs were made on anesthetized fish immobilized into a wet foam holder. PD166866 (Merck- PZ0114) was dissolved in DMSO at a stock concentration of 25 mM. It was diluted in PBS and injected intraperitoneally at 370 µg/gm body weight. Cyclopamine (Merck- C4116) was dissolved in DMSO at a stock concentration of 10 mM. The stock was diluted in PBS and injected intraperitoneally at 41.3 µg/gm body weight. The injection volume of the chemical or DMSO (vehicle control) was adjusted to 10 µl with 1X PBS and injected intraperitoneally/day for 4 days. SU5402 (Merck- SML0443) was dissolved in DMSO at a stock concentration of 17 mM. The inhibitor was added to the system water at a volume to make the working concentration of 17µM, and the same volume of DMSO was added as vehicle control. 4 animals were maintained in 100 ml system water with DMSO or SU5402. Animals received fresh treatment every 24 h for 3 days. Control and treated animals were maintained in separate tanks during the experiment. Animals were sacrificed 24 h after the last injection and processed for qPCR or histological analysis.

Confocal microscopy

Stained tissue sections were imaged with a Leica SP8 confocal laser scanning microscope (Leica Microsystems, Germany), keeping all the parameters fixed for scanning the test and control samples. The acquired confocal z-stacks were processed and analyzed with LAS X (Leica) or GIMP (GIMP Development Team) software.

Protein interaction assay

Proximity ligation assay (PLA) was performed to identify the interaction between zebrafish Ccn2a and Fgfr1a or Fgfr1b. C-terminal Myc-tagged full-length *ccn2a* (Ccn2a-FL^{Myc}), C-terminal Myc-tagged N-terminal fragment of *ccn2a* (Ccn2a-NTF^{Myc}), C-terminal FLAG-tagged full-length *fgfr1a* (Fgfr1a^{FLAG}), and C-terminal FLAG-tagged full-length *fgfr1b* (Fgfr1b^{FLAG}) mRNAs were synthesized using linearized FL-Z*ccn2a*-MYC, NTF-Z*ccn2a*-MYC, FL-Z*fgfr1a*-FLAG, and FL-Z*fgfr1b*-FLAG, respectively and mMESSAGE mMACHINE™ SP6 Transcription Kit (ThermoFisher Scientific- AM1340) as per manufacturer's instructions. *In vitro* synthesized mRNAs of Ccn2a-FL^{Myc} or Ccn2a-NTF^{Myc} were co-injected with Fgfr1a^{FLAG} or Fgfr1b^{FLAG} mRNA in 1-cell stage embryos. Embryos were harvested at 30 hpf, fixed in 4% PFA in PBS overnight at 4^{o}C. Around 50% of the fixed embryos were processed for immunostaining, and the remaining embryos were processed for the proximity ligation assay (PLA).

Whole-mount immunostaining was performed on 30 hpf fixed embryos to detect the expression of injected tagged mRNAs. Fixed embryos were washed thrice in PBS, permeabilized with 0.5% Triton X-100 in PBS, and blocked for 1h in blocking solution (5% goat serum (MP Biomedicals) and 0.5% Triton X-100 in PBS). Subsequently, embryos were incubated with primary antibodies [mouse, anti-Myc, 1:250 (Merck- M4439) and rabbit, anti-FLAG, 1:250 (Cell Signaling Technologies- 14793S)]. Primary immune complexes were detected using goat, anti-mouse Alexa Flour™ 488- (Thermo Fisher Scientific- A21042), and goat, anti-rabbit Alexa Flour™ 647- (Thermo Fisher Scientific- A32733) conjugated secondary antibodies (1:400). DAPI (1 µg/mL in PBS) was used to detect nuclei. For imaging, embryos were flat-mounted in Mowiol® 4-88 Reagent (Merck) and imaged with a Leica SP8 confocal laser scanning microscope.

After confirmation of the expression of the injected mRNAs, PLA was performed on the rest injected clutch mates using Duolink® In Situ Orange Starter Kit Mouse/Rabbit (Merck-DUO92102) as per the manufacturer's instruction. In brief, fixed embryos were processed and treated with the primary antibodies similar to the above-mentioned whole-mount immunostaining. The next day embryos were washed in buffer-A twice for 5 mins each at RT and incubated with the PLA probe solution for 1 h at 37°C. Subsequently, embryos were washed in buffer-A twice for 5 minutes each at RT and incubated in the ligation solution for 30 minutes at 37°C. Further, embryos were washed in buffer-A twice for 5 minutes each at RT and incubated in amplification solution for 100 minutes at 37°C. After washing in buffer-B twice for 10 mins each at RT, embryos were incubated in DAPI (1 µg/mL PBS, Merck) to detect nuclei. Embryos were flat-mounted on a glass slide in Duolink® In Situ Mounting medium, and optical sections were captured with a Leica SP8 confocal laser scanning microscope, and images were processed with LAS X (Leica) or GIMP.

Statistical analysis

The Student's T-test was performed to analyze statistical differences in gene expression, cell proliferation indices, and cell death indices. Statistical significance was considered at $p<0.05$ for all analyses. Data were processed with the GraphPad Prism7 software. Values are represented as the mean ± s.e.m.

ACKNOWLEDGMENTS

We are grateful to Kenneth D. Poss for providing Tg(*hsp70*:ca-fgfr1) transgenic zebrafish and Mahendra Sonawane for critical reading of the manuscript. We thank Satish Bojja for the excellent fish care and ARI for internal support.

Declaration of interests

The authors declare no competing interests.

Author contributions

Conceptualization: AR, CP; Methodology: AR, GW (Microinjection), CP; Validation: AR; Formal analysis: AR; Investigation: AR, CP; Resources: MS, CP; Data curation: AR; Writing – original draft: AR, CP; Writing – review & editing: AR, MS, CP; Visualization: AR, CP; Supervision: CP; Funding acquisition: CP

Funding

This work was supported by the DBT/Wellcome Trust India Alliance Intermediate Fellowship (Ref# IA/I/18/2/504016) to CP and a Ph.D. fellowship from DBT, New Delhi to AR.

REFERENCES

Aleström, P., D'Angelo, L., Midtlyng, P. J., Schorderet, D. F., Schulte-Merker, S., Sohm, F. and Warner, S. (2020). Zebrafish: Housing and husbandry recommendations. *Lab Anim* **54**, 213–224.

Bedore, J., Sha, W., McCann, M. R., Liu, S., Leask, A. and Séguin, C. A. (2013). Impaired intervertebral disc development and premature disc degeneration in mice with notochord-specific deletion of CCN2. *Arthritis Rheum* **65**, 2634–44.

Bonifas, J. M., Pennypacker, S., Chuang, P. T., McMahon, A. P., Williams, M., Rosenthal, A., de Sauvage, F. J. and Epstein, E. H. (2001). Activation of expression of hedgehog target genes in basal cell carcinomas. *Journal of Investigative Dermatology* **116**, 739–742.

Buckwalter, J. A. (1995). Aging and degeneration of the human intervertebral disc. *Spine (Phila Pa 1976)* **20**, 1307–14.

Cermak, T., Starker, C. G. and Voytas, D. F. (2015). Efficient design and assembly of custom TALENs using the Golden Gate platform. *Methods Mol Biol* **1239**, 133–59.

Cheung, K. M. C., Karppinen, J., Chan, D., Ho, D. W. H., Song, Y. Q., Sham, P., Cheah, K. S. E., Leong, J. C. Y. and Luk, K. D. K. (2009). Prevalence and pattern of lumbar magnetic resonance imaging changes in a population study of one thousand forty-three individuals. *Spine (Phila Pa 1976)* **34**, 934–940.

Choi, K.-S. and Harfe, B. D. (2011). Hedgehog signaling is required for formation of the notochord sheath and patterning of nuclei pulposi within the intervertebral discs. *Proc Natl Acad Sci U S A* **108**, 9484–9.

Chuang, P. T., Kawcak, T. and McMahon, A. P. (2003). Feedback control of mammalian Hedgehog signaling by the Hedgehog-binding protein, Hip1, modulates Fgf signaling during branching morphogenesis of the lung. *Genes Dev* **17**, 342–347.

Dahia, C. L., Mahoney, E. J., Durrani, A. A. and Wylie, C. (2009). Postnatal growth, differentiation, and aging of the mouse intervertebral disc. *Spine (Phila Pa 1976)* **34**, 447–55.

Dahia, C. L., Mahoney, E. and Wylie, C. (2012). Shh signaling from the nucleus pulposus is required for the postnatal growth and differentiation of the mouse intervertebral disc. *PLoS One* **7**, e35944.

DeSalvo, J., Ban, Y., Li, L., Sun, X., Jiang, Z., Kerr, D. A., Khanlari, M., Boulina, M., Capecchi, M. R., Partanen, J. M., et al. (2021). ETV4 and ETV5 drive synovial sarcoma through cell cycle and DUX4 embryonic pathway control. *Journal of Clinical Investigation* **131**,.

Eskola, P. J., Kjaer, P., Daavittila, I. M., Solovieva, S., Okuloff, A., Sorensen, J. S., Wedderkopp, N., Ala-Kokko, L., Männikkö, M. and Karppinen, J. I. (2010). Genetic risk factors of disc degeneration among 12-14-year-old Danish children: a population study. *Int J Mol Epidemiol Genet* **1**, 158–65.

Fernando, C. A., Conrad, P. A., Bartels, C. F., Marques, T., To, M., Balow, S. A., Nakamura, Y. and Warman, M. L. (2010). Temporal and spatial expression of CCN genes in zebrafish. *Dev Dyn* **239**, 1755–67.

Garcia, J., Bagwell, J., Njaine, B., Norman, J., Levic, D. S., Wopat, S., Miller, S. E., Liu, X., Locasale, J. W., Stainier, D. Y. R., et al. (2017). Sheath Cell Invasion and Trans-differentiation Repair Mechanical Damage Caused by Loss of Caveolae in the Zebrafish Notochord. *Curr Biol* **27**, 1982-1989.e3.

Grotendorst, G. R. and Duncan, M. R. (2005). Individual domains of connective tissue growth factor regulate fibroblast proliferation and myofibroblast differentiation. *FASEB J* **19**, 729–38.

Haga, Y., Dominique, V. J. and Du, S. J. (2009). Analyzing notochord segmentation and intervertebral disc formation using the twhh:gfp transgenic zebrafish model. *Transgenic Res* **18**, 669–83.

Hashizume, H. (1980). Three-dimensional architecture and development of lumber intervertebral discs. *Acta Med Okayama* **34**, 301–314.

Henriksson, H. B., Thornemo, M., Karlsson, C., Hägg, O., Junevik, K., Lindahl, A. and Brisby, H. (2009). Identification of Cell Proliferation Zones, Progenitor Cells and a Potential Stem Cell Niche in the Intervertebral Disc Region. *Spine (Phila Pa 1976)* **34**, 2278–2287.

Hollenberg, A. M., Maqsoodi, N., Phan, A., Huber, A., Jubril, A., Baldwin, A. L., Yokogawa, N., Eliseev, R. A. and Mesfin, A. (2021). Bone morphogenic protein-2 signaling in human disc

degeneration and correlation to the Pfirrmann MRI grading system. *The Spine Journal* **21**, 1205–1216.

Incardona, J. P., Gaffield, W., Kapur, R. P. and Roelink, H. (1998). The teratogenic Veratrum alkaloid cyclopamine inhibits Sonic hedgehog signal transduction. *Development* **125**, 3553–3562.

Ivkovic, S., Yoon, B. S., Popoff, S. N., Safadi, F. F., Libuda, D. E., Stephenson, R. C., Daluiski, A. and Lyons, K. M. (2003). Connective tissue growth factor coordinates chondrogenesis and angiogenesis during skeletal development. *Development* **130**, 2779–91.

Jaffa, A. A., Usinger, W. R., McHenry, M. B., Jaffa, M. A., Lipstiz, S. R., Lackland, D., Lopes-Virella, M., Luttrell, L. M., Wilson, P. W. F. and Diabetes Control and Complications Trial/Epidemiology of Diabetes Interventions and Complications Study Group (2008). Connective tissue growth factor and susceptibility to renal and vascular disease risk in type 1 diabetes. *J Clin Endocrinol Metab* **93**, 1893–900.

Kague, E., Turci, F., Newman, E., Yang, Y., Brown, K. R., Aglan, M. S., Otaify, G. A., Temtamy, S. A., Ruiz-Perez, V. L., Cross, S., et al. (2021). 3D assessment of intervertebral disc degeneration in zebrafish identifies changes in bone density that prime disc disease. *Bone Res* **9**, 39.

Kessel, M. and Gruss, P. (1991). Homeotic transformations of murine vertebrae and concomitant alteration of Hox codes induced by retinoic acid. *Cell* **67**, 89–104.

Koziczak, M., Holbro, T. and Hynes, N. E. (2004). Blocking of FGFR signaling inhibits breast cancer cell proliferation through downregulation of D-type cyclins. *Oncogene* **23**, 3501–3508.

Lavine, K. J. (2006). Fibroblast growth factor signals regulate a wave of Hedgehog activation that is essential for coronary vascular development. *Genes Dev* **20**, 1651–1666.

Lepilina, A., Coon, A. N., Kikuchi, K., Holdway, J. E., Roberts, R. W., Burns, C. G. and Poss, K. D. (2006). A Dynamic Epicardial Injury Response Supports Progenitor Cell Activity during Zebrafish Heart Regeneration. *Cell* **127**, 607–619.

Li, X., An, H. S., Ellman, M., Phillips, F., Thonar, E. J., Park, D. K., Udayakumar, R. K. and Im, H.-J. (2008). Action of fibroblast growth factor-2 on the intervertebral disc. *Arthritis Res Ther* **10**, R48.

Litingtung, Y., Lei, L., Westphal, H. and Chiang, C. (1998). Sonic hedgehog is essential to foregut development. *Nat Genet* **20**, 58–61.

Lleras Forero, L., Narayanan, R., Huitema, L. F., VanBergen, M., Apschner, A., Peterson-Maduro, J., Logister, I., Valentin, G., Morelli, L. G., Oates, A. C., et al. (2018). Segmentation of the zebrafish axial skeleton relies on notochord sheath cells and not on the segmentation clock. *Elife* **7**,.

Marques, S. R., Lee, Y., Poss, K. D. and Yelon, D. (2008). Reiterative roles for FGF signaling in the establishment of size and proportion of the zebrafish heart. *Dev Biol* **321**, 397–406.

Matta, A., Karim, M. Z., Isenman, D. E. and Erwin, W. M. (2017). Molecular Therapy for Degenerative Disc Disease: Clues from Secretome Analysis of the Notochordal Cell-Rich Nucleus Pulposus. *Sci Rep* **7**, 45623.

Mohammadi, M., McMahon, G., Sun, L., Tang, C., Hirth, P., Yeh, B. K., Hubbard, S. R. and Schlessinger, J. (1997). Structures of the Tyrosine Kinase Domain of Fibroblast Growth Factor Receptor in Complex with Inhibitors. *Science (1979)* **276**, 955–960.

Mokalled, M. H., Patra, C., Dickson, A. L., Endo, T., Stainier, D. Y. R. and Poss, K. D. (2016). Injury-induced ctgfa directs glial bridging and spinal cord regeneration in zebrafish. *Science* **354**, 630–634.

Mori, T., Kawara, S., Shinozaki, M., Hayashi, N., Kakinuma, T., Igarashi, A., Takigawa, M., Nakanishi, T. and Takehara, K. (1999). Role and interaction of connective tissue growth factor with transforming growth factor-beta in persistent fibrosis: A mouse fibrosis model. *J Cell Physiol* **181**, 153–9.

Mukherjee, D., Wagh, G., Mokalled, M. H., Kontarakis, Z., Dickson, A. L., Rayrikar, A., Günther, S., Poss, K. D., Stainier, D. Y. R. and Patra, C. (2021). Ccn2a is an injury-induced matricellular factor that promotes cardiac regeneration in zebrafish. *Development* **148**,.

Oegema, T. R., Johnson, S. L., Aguiar, D. J. and Ogilvie, J. W. (2000). Fibronectin and its fragments increase with degeneration in the human intervertebral disc. *Spine (Phila Pa 1976)* **25**, 2742–7.

Panek, R. L., Lu, G. H., Dahring, T. K., Batley, B. L., Connolly, C., Hamby, J. M. and Brown, K. J. (1998). In vitro biological characterization and antiangiogenic effects of PD 166866, a selective inhibitor of the FGF-1 receptor tyrosine kinase. *J Pharmacol Exp Ther* **286**, 569–77.

Patra, C., Kontarakis, Z., Kaur, H., Rayrikar, A., Mukherjee, D. and Stainier, D. Y. R. (2017). The zebrafish ventricle: A hub of cardiac endothelial cells for in vitro cell behavior studies. *Sci Rep* **7**, 2687.

Pearce, R. H., Grimmer, B. J. and Adams, M. E. (1987). Degeneration and the chemical composition of the human lumbar intervertebral disc. *J Orthop Res* **5**, 198–205.

Peng, B., Chen, J., Kuang, Z., Li, D., Pang, X. and Zhang, X. (2009). Expression and role of connective tissue growth factor in painful disc fibrosis and degeneration. *Spine (Phila Pa 1976)* **34**, E178-82.

Riley, K. G., Pasek, R. C., Maulis, M. F., Peek, J., Thorel, F., Brigstock, D. R., Herrera, P. L. and Gannon, M. (2015). Connective tissue growth factor modulates adult β-cell maturity and proliferation to promote β-cell regeneration in mice. *Diabetes* **64**, 1284–98.

Robinson, P. M., Smith, T. S., Patel, D., Dave, M., Lewin, A. S., Pi, L., Scott, E. W., Tuli, S. S. and Schultz, G. S. (2012). Proteolytic processing of connective tissue growth factor in normal ocular tissues and during corneal wound healing. *Invest Ophthalmol Vis Sci* **53**, 8093–103.

Roughley, P. J. (2004). Biology of intervertebral disc aging and degeneration: involvement of the extracellular matrix. *Spine (Phila Pa 1976)* **29**, 2691–9.

Rufai, A., Benjamin, M. and Ralphs, J. R. (1995). The development of fibrocartilage in the rat intervertebral disc. *Anat Embryol (Berl)* **192**, 53–62.

Tamatani, T., Kobayashi, H., Tezuka, K., Sakamoto, S., Suzuki, K., Nakanishi, T., Takigawa, M. and Miyano, T. (1998). Establishment of the enzyme-linked immunosorbent assay for connective tissue growth factor (CTGF) and its detection in the sera of biliary atresia. *Biochem Biophys Res Commun* **251**, 748–52.

Teraguchi, M., Yoshimura, N., Hashizume, H., Yamada, H., Oka, H., Minamide, A., Nagata, K., Ishimoto, Y., Kagotani, R., Kawaguchi, H., et al. (2017). Progression, incidence, and risk factors for intervertebral disc degeneration in a longitudinal population-based cohort: the Wakayama Spine Study. *Osteoarthritis Cartilage* **25**, 1122–1131.

Trefilova, V. V., Shnayder, N. A., Petrova, M. M., Kaskaeva, D. S., Tutynina, O. V., Petrov, K. V., Popova, T. E., Balberova, O. V., Medvedev, G. V. and Nasyrova, R. F. (2021). The Role of Polymorphisms in Collagen-Encoding Genes in Intervertebral Disc Degeneration. *Biomolecules* **11**, 1279.

Verheyden, J. M., Lewandoski, M., Deng, C., Harfe, B. D. and Sun, X. (2005). Conditional inactivation of Fgfr1 in mouse defines its role in limb bud establishment, outgrowth and digit patterning. *Development* **132**, 4235–4245.

Winkler, T., Mahoney, E. J., Sinner, D., Wylie, C. C. and Dahia, C. L. (2014). Wnt signaling activates Shh signaling in early postnatal intervertebral discs, and re-activates Shh signaling in old discs in the mouse. *PLoS One* **9**, e98444.

Wopat, S., Bagwell, J., Sumigray, K. D., Dickson, A. L., Huitema, L. F. A., Poss, K. D., Schulte-Merker, S. and Bagnat, M. (2018). Spine Patterning Is Guided by Segmentation of the Notochord Sheath. *Cell Rep* **22**, 2026–2038.

Wu, Q., Mathers, C., Wang, E. W., Sheng, S., Wenkert, D. and Huang, J. H. (2019). TGF-β Initiates β-Catenin-Mediated CTGF Secretory Pathway in Old Bovine Nucleus Pulposus Cells: A Potential Mechanism for Intervertebral Disc Degeneration. *JBMR Plus* **3**, e10069.

Yan, N., Yu, S., Zhang, H. and Hou, T. (2015). Lumbar Disc Degeneration is Facilitated by MiR-100-Mediated FGFR3 Suppression. *Cell Physiol Biochem* **36**, 2229–36.

Figures

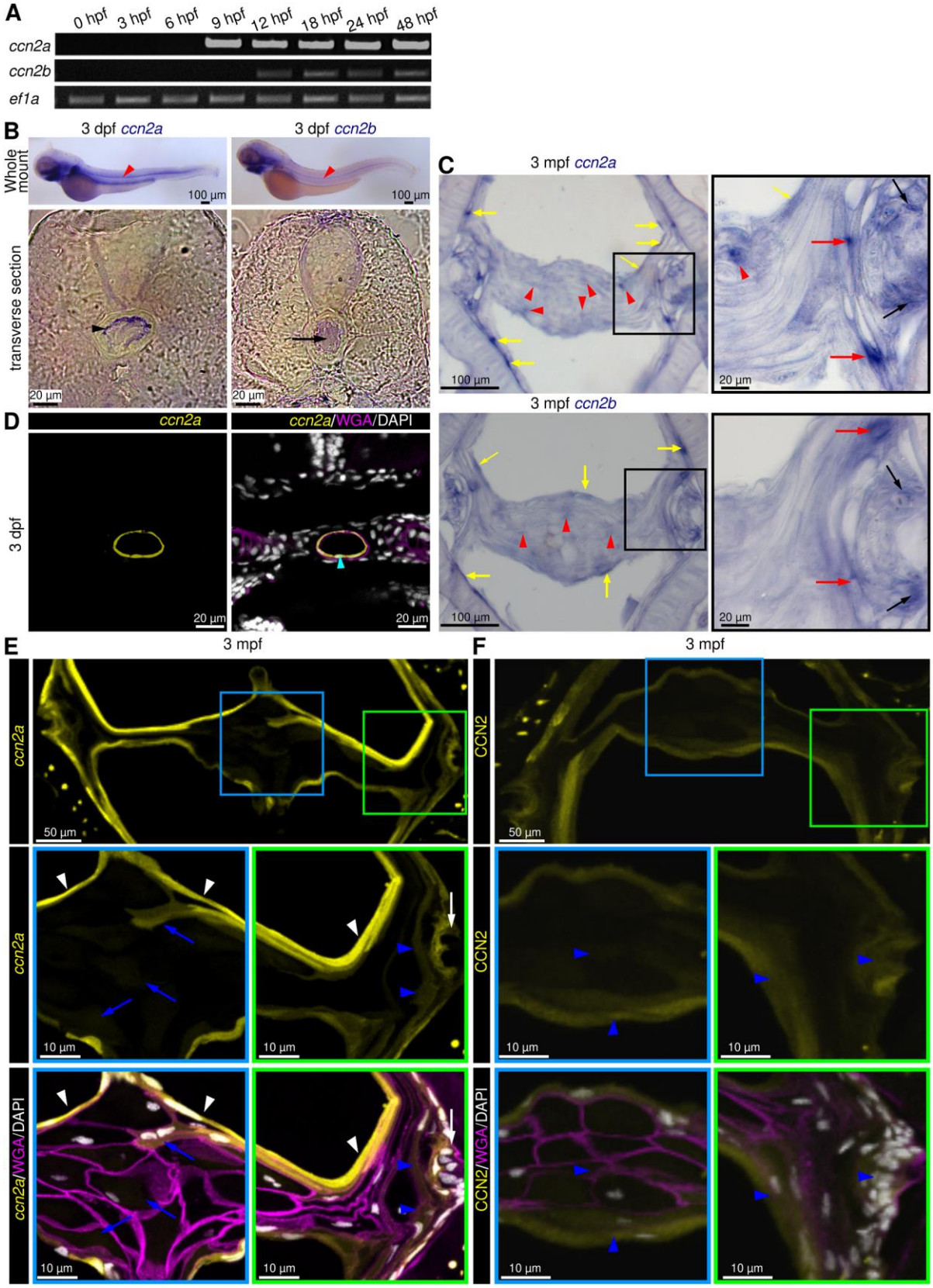

Fig. 1. *ccn2a* and *ccn2b* are expressed in larval notochord and adult IVDs. (A) Semi-qPCR analysis of *ccn2a* and *ccn2b* in zebrafish embryos. *ef1α* is loading control. (B) Bright-field images of whole-mount *in situ* hybridized embryos and their transverse sections. Red arrowheads indicate *ccn2a* or *ccn2b* expression in the notochord. Black arrowhead and arrow show *ccn2a* transcripts in the NSCs, and *ccn2b* transcripts in the NCs, respectively. (C) *ccn2a* and *ccn2b* expression on sagittal sections of IVD. Black, red, and yellow arrows indicate *ccn2a* or *ccn2b* expressing cells in the OAF, IAF, and NSCs, respectively. Red arrowheads show weak *ccn2a* and *ccn2b* expression in the NP cells. (D) *BACccn2a*:EGFP expression (yellow) in a transverse section of a 3 dpf embryo stained with WGA (magenta; cell membrane) and DAPI (white; nuclei). Arrowhead indicates EGFP expression in the NSCs. (E) *BACccn2a*:EGFP expression (yellow) in a sagittal section of IVD stained with wheat germ agglutinin (magenta; cell membrane) and DAPI (white; nuclei). White arrows and arrowheads indicate EGFP expression in OAF and sheath cells, respectively. Blue arrows and arrowheads indicate weak EGFP expression in NP and IAF cells, respectively. (F) Maximum intensity projections of confocal images of a sagittal section of IVD immunostained for Ccn2 (yellow), stained with WGA (magenta; cell membrane), and DAPI (white; nuclei). Arrowheads indicate ubiquitous localization of Ccn2 throughout the IVD.

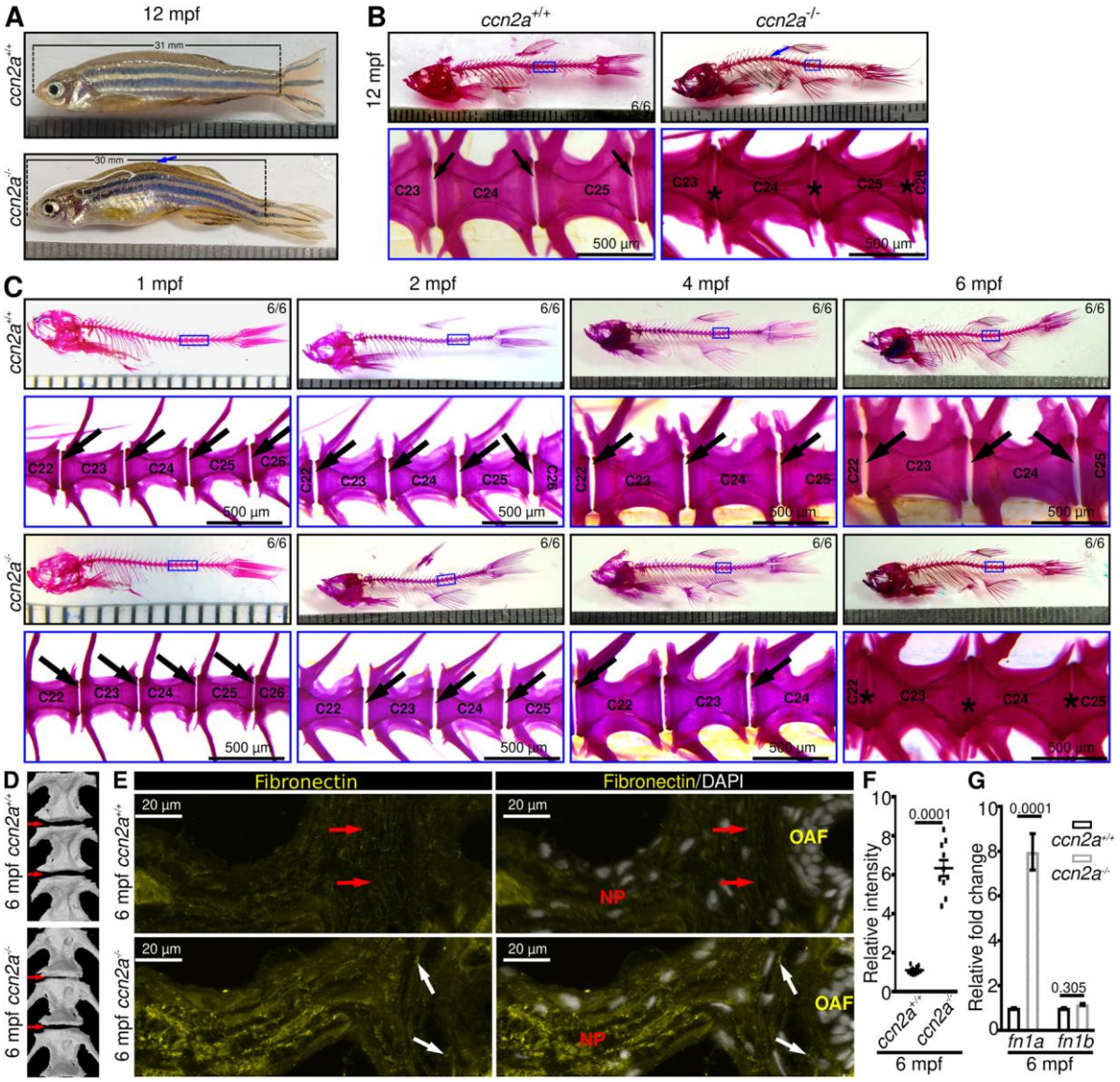

Fig. 2. *ccn2a*$^{-/-}$ exhibits IVDD in adult zebrafish. (A) Bright-field images. Arrow indicates the curvature in the body axis of *ccn2a*$^{-/-}$. mm; millimeter. (B, C) Bright-field images of whole-mount AB/AR stained animals. Blue arrows in (B) indicate the curvature in the spine of *ccn2a*$^{-/-}$. Black arrows indicate intervertebral gaps, which are not visible in *ccn2a*$^{-/-}$ at 6 mpf. (D) µCT images of zebrafish spine. Arrows indicate the intervertebral region. (E) Maximum intensity projections of confocal images of IVD sagittal sections immunostained for fibronectin (yellow) and stained with DAPI (white; nuclei). Red and white arrows indicate striated and fragmented fibronectin expression in the IAF of the WT and *ccn2a*$^{-/-}$ IVD, respectively. Increased fibronectin expression is visible in the *ccn2a*$^{-/-}$ IVD. (F) Quantification of E (n=10). The mean of the WT control value was set to 1. (G)

Quantification of *fn1a* and *fn1b* expression in vertebral tissues (n=4). Mean Ct values-Table S5.

In F and G, data are measured mean ± s.e.m. and each sample represents one animal. Digits on the images in B and C indicate the number of fish that showed the presented phenotype out of how many fish. 'C' on images in B and C represent centrum/vertebrae.

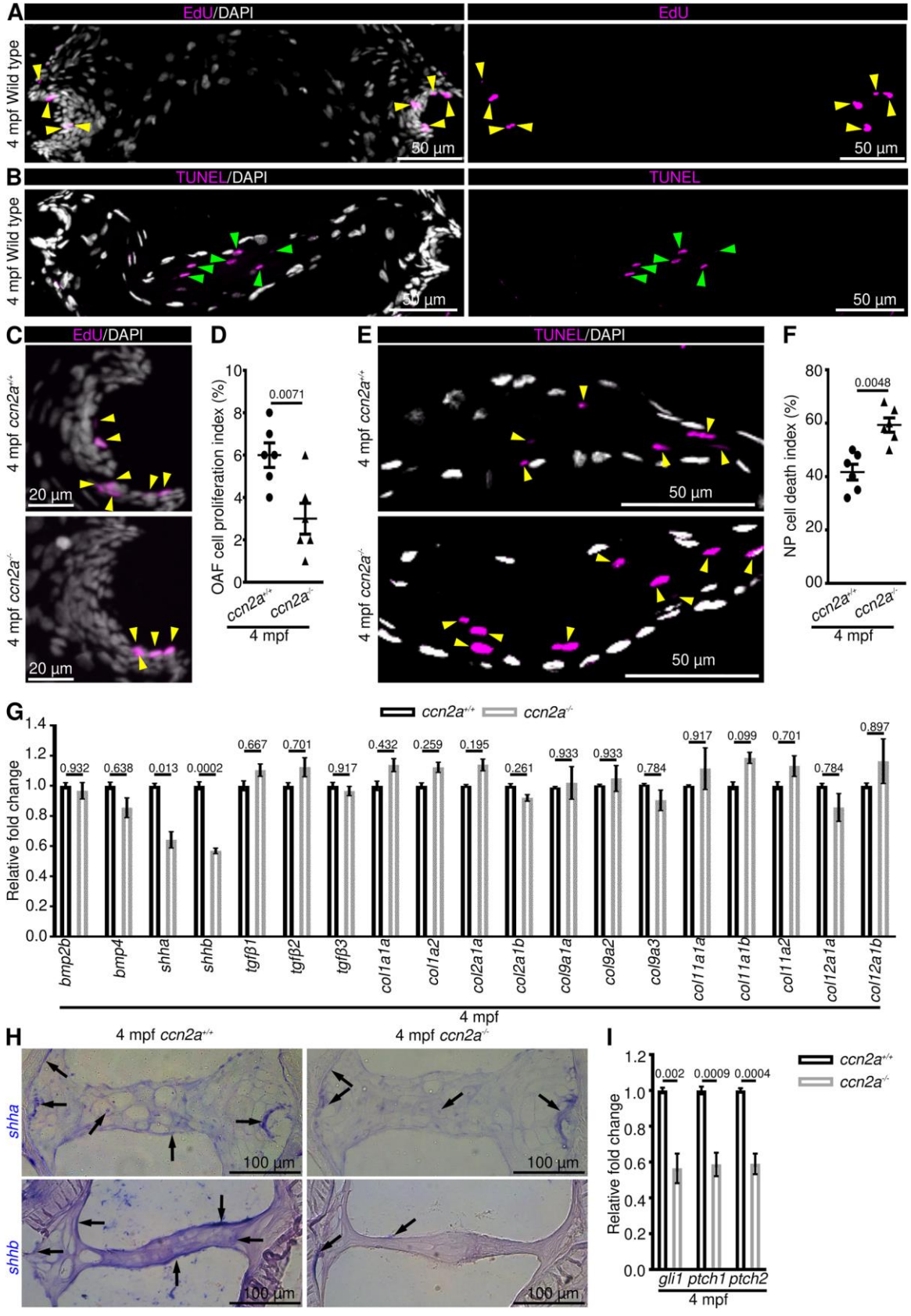

Fig. 3. Adult *ccn2a*$^{-/-}$ display decreased OAF cell proliferation, increased NP cell death, and decreased SHH signaling. (A, B) MIPs of confocal images of sagittal IVD sections stained for EdU (magenta; proliferating cells) and nuclei (white; DAPI) (A) or stained for TUNEL (magenta; dead cells) and nuclei (white; DAPI) (B). Yellow and green arrowheads indicate EdU^{+} OAF cells and TUNEL^{+} NP cells, respectively. (C) MIPs of confocal images of sagittal IVD sections stained for EdU (magenta; proliferating cells) and stained with DAPI (white; nuclei). Arrowheads indicate EdU^{+} cells. (D) Quantification of OAF cell proliferation (n=6). (E) MIPs of confocal images of IVD sagittal sections stained for TUNEL (magenta; dead cells) and stained with DAPI (white; nuclei). Arrowheads indicate TUNEL^{+} NP cells. (F) Quantification of NP cell death (n=6). (G) qPCR to identify differentially expressed genes in 4 mpf *ccn2a*$^{-/-}$ vertebral tissues (n=4). (H) *shha* and *shhb* expression on sagittal sections of IVD. Arrows indicate mRNA expression. (I) Quantification of *gli1*, *ptch1*, and *ptch2* expression in vertebral tissues (n=4). In D, F, G, and I, data are mean ± s.e.m. and each sample represents one animal; MIP, maximum intensity projection. Mean Ct values-Table S5.

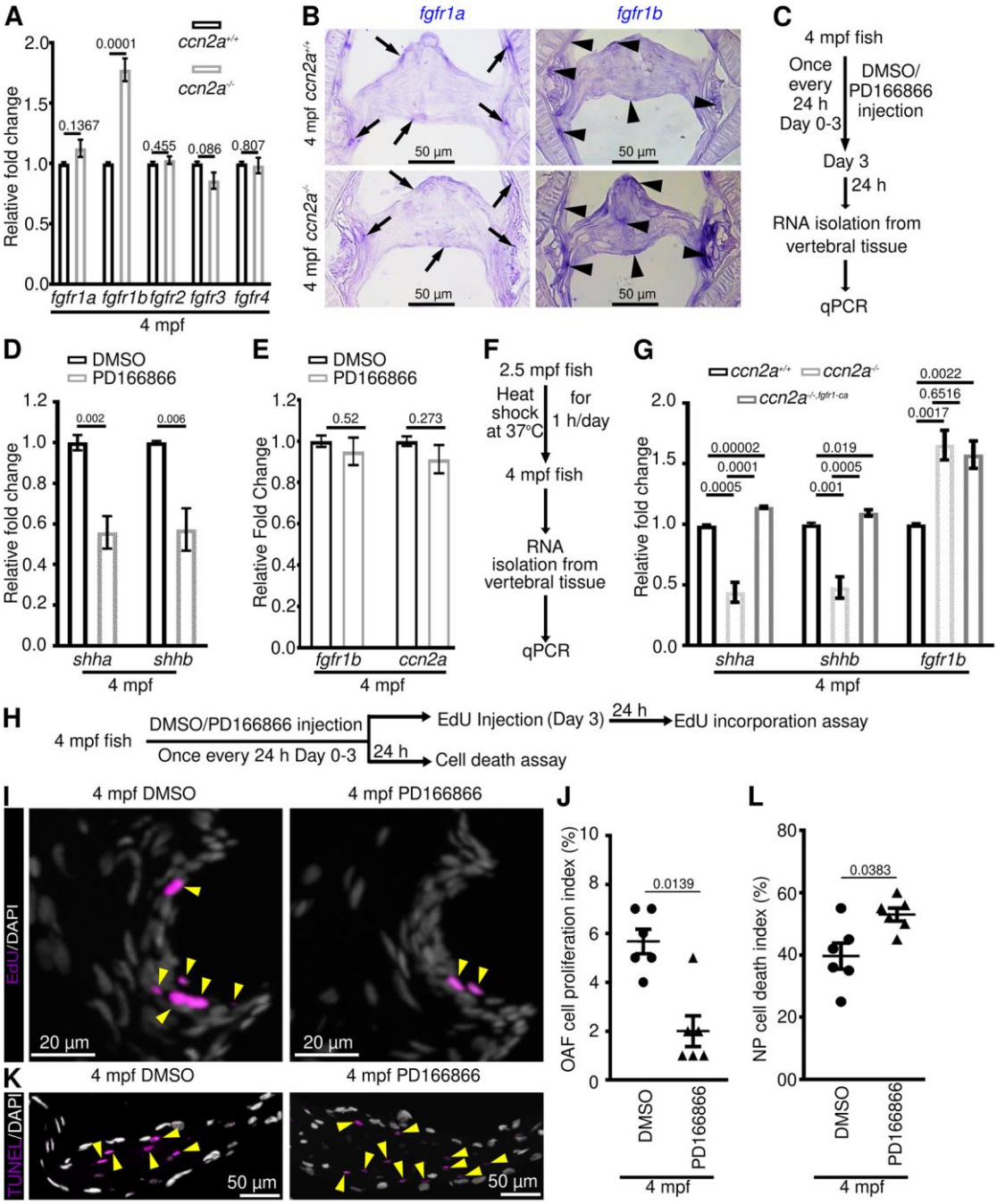

Fig. 4. FGFR1 signaling regulates *shha* and *shhb* expression, OAF cell proliferation, and NP cell survival in adult IVDs. (A) Quantification of FGFRs expression in vertebral tissues (n=4). (B) *fgfr1a* and *fgfr1b* expression on sagittal sections of IVD. (C) Schematic of experimental procedures. (D, E) qPCR analysis of *shha* and *shhb* (D) and *fgfr1b* and *ccn2a* (E) expression in vertebral tissues (n=4). (F) Schematic of experimental procedures. (G) qPCR analysis of *shha*, *shhb*, and *fgfr1b* expression in vertebral tissues (n=4). (H) Schematic of experimental procedures. (I) MIPs of confocal images of sagittal IVD sections stained for EdU (magenta; proliferating cells) and stained with DAPI (white; nuclei). Arrowheads

indicate EdU^+ OAF cells. (J) Quantification of proliferating OAF cell (n=6). (K) MIPs of confocal images of sagittal IVD sections stained for TUNEL (magenta; dead cells) and stained with DAPI (white; nuclei). Arrowheads indicate $TUNEL^+$ NP cells. (L) Dot plot showing the percentage of $TUNEL^+$ NP cells (n=6).

In A, D, E, G, J, and L, data are mean ± s.e.m. and each sample represents one animal; MIP maximum intensity projections. Mean Ct values-Table S5.

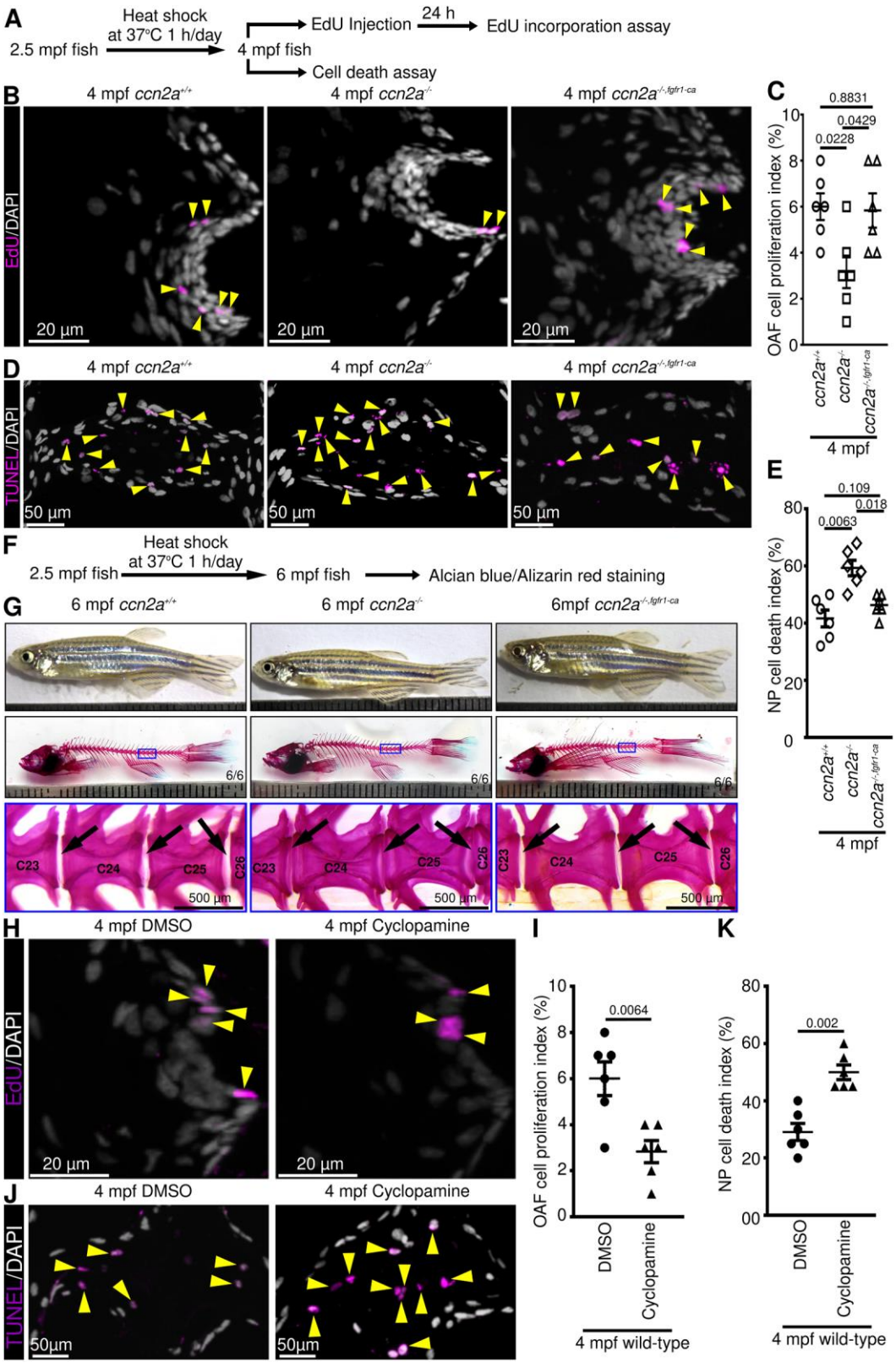

Fig. 5. Ectopic expression of a constitutively active form of Fgfr1 can restore cellular phenotype in adult *ccn2a*$^{-/-}$ IVDs through SHH signaling. (A) Schematic depiction of experimental procedures. (B) MIPs of confocal images of sagittal IVD sections stained for

EdU (magenta; proliferating cells) and nuclei (white). Arrowheads indicate EdU^+ cells in the OAF. (C) Quantification of proliferating OAF cell (n=6). (D) MIPs of confocal images of sagittal IVD sections stained for TUNEL (magenta; dead cells) and nuclei (white). Arrowheads indicate $TUNEL^+$ cells in the NP. (E) Quantification of NP cell death (n=6). (F) Schematic depiction of experimental procedures. (G) Bright-field lateral views of live and AB/AR stained zebrafish. Black arrows indicate intervertebral spaces. mm; millimeter. (H) MIPs of confocal images of sagittal IVD sections stained for EdU (magenta; proliferating cells) and stained with DAPI (white; nuclei). Arrowheads indicate EdU^+ cells in the OAF. (I) Quantification of proliferating OAF cell (n=6). (J) MIPs of confocal images of sagittal IVD sections stained for TUNEL (magenta; dead cells) and nuclei (white). Arrowheads indicate $TUNEL^+$ cells in the NP. (K) Quantification of NP cell death (n=6).

In C, E, I, and K, data are mean ± s.e.m. and each sample represents one animal. Digits on the images in G indicate the number of fish that showed the presented phenotype out of how many fish. MIP, maximum intensity projection. 'C' on images in G represents centrum/vertebrae.

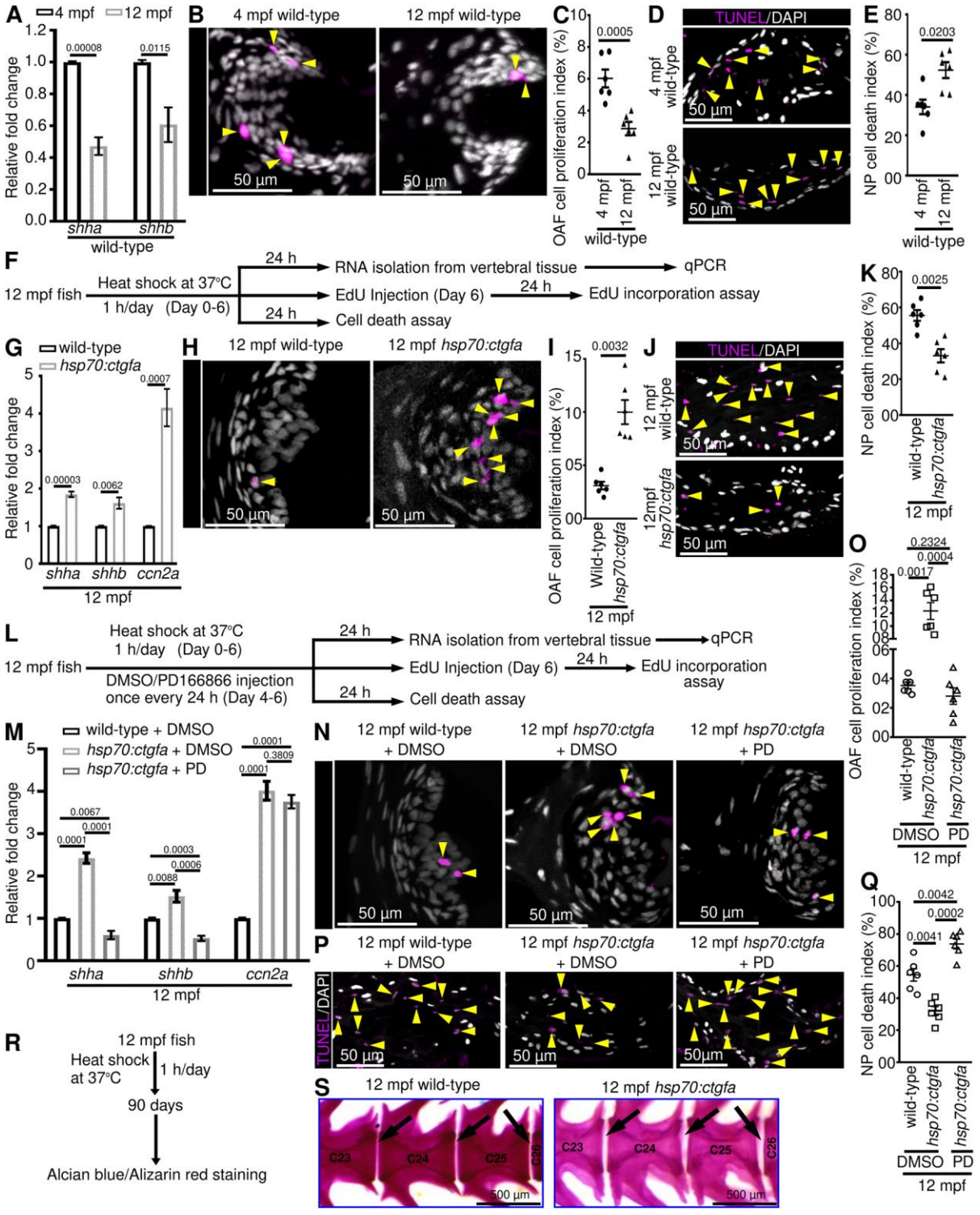

Fig. 6. Ccn2a induces regeneration in aged IVDs by inducing FGFR1 signaling. (A) qPCR analysis of *shha* and *shhb* expression in vertebral tissues (n=4). (B) MIPs of confocal images of sagittal IVD sections stained for EdU (magenta; proliferating cells) and nuclei (white). Arrowheads indicate EdU^{+} cells in the OAF. (C) Quantification of proliferating OAF cell (n=6 each). (D) MIPs of confocal images of sagittal IVD sections stained for

TUNEL (magenta; dead cells) and nuclei (white). Arrowheads indicate TUNEL^{+} cells in the NP. (E) Quantification of NP cell death (n=6). (F) Schematic of experimental procedures. (G) qPCR analysis of *shha*, *shhb*, and *ccn2a* expression in vertebral tissues (n=4). (H) MIPs of confocal images of sagittal IVD sections stained for EdU (magenta; proliferating cells) and nuclei (white). Arrowheads indicate EdU^{+} cells in the OAF. (I) Quantification of proliferating OAF cell (n=6). (J) MIPs of confocal images of sagittal IVD sections stained for TUNEL (magenta; dead cells) and nuclei (white). Arrowheads indicate TUNEL^{+} cells in the NP. (K) Quantification of NP cell death (n=6). (L) Schematic of experimental procedures. (M) qPCR analysis of *shha*, *shhb*, and *ccn2a* expression in vertebral tissues (n=4). (N) MIPs of confocal images of sagittal IVD sections stained for EdU (magenta; proliferating cells) and nuclei (white). Arrowheads indicate EdU^{+} cells in the OAF. (O) Quantification of proliferating OAF cell (n=6). (P) MIPs of confocal images of sagittal IVD sections stained for TUNEL (magenta; dead cells) and nuclei (white). Arrowheads indicate TUNEL^{+} cells in the NP. (Q) Quantification of NP cell death (n=6). (R) Schematic of experimental procedures. (S) Bright-field lateral views of AB/AR-stained zebrafish. Black arrows indicate intervertebral spaces. mm; millimeter.

In A, C, E, G, I, K, M, O, and Q, data are mean ± s.e.m. and each sample represents one animal; MIP, maximum intensity projection; PD, PD166866. Mean Ct values-Table S5.

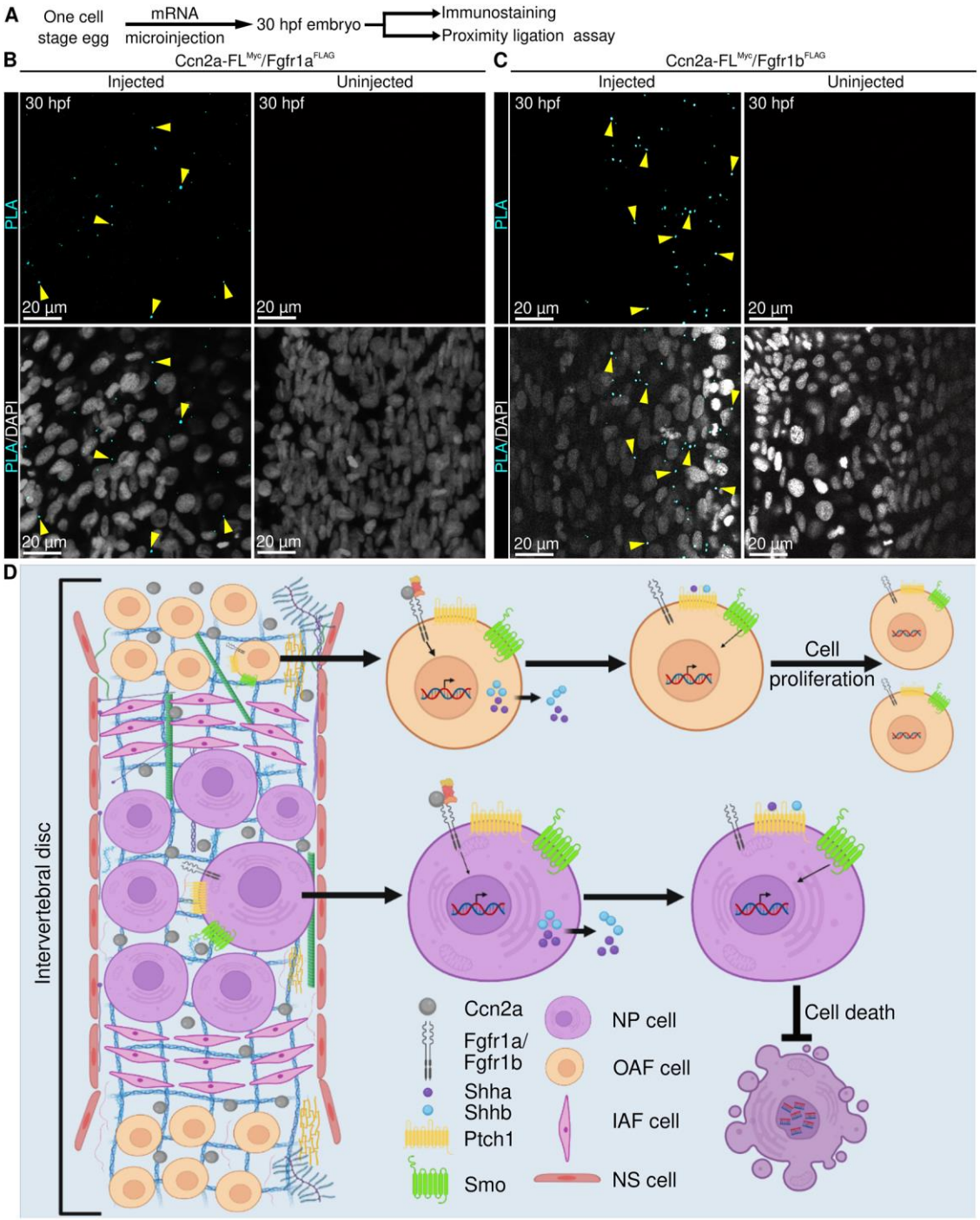

Fig. 7. Ccn2a interacts with Fgfr1a and Fgfr1b *in vivo*. (A) Schematic of experimental procedures. (B, C) Representative single plane optical sections of whole-mount 30 hpf embryos stained for proximity detection (cyan, interacting complex) and nuclei (white). Arrowheads in (B) indicate an interaction between C-terminal Myc-tagged Ccn2a and N-terminal FLAG-tagged Fgfr1a (cyan). Arrows in (C) indicate an interaction between N-terminal Myc-tagged Ccn2a and N-terminal FLAG-tagged Fgfr1b (cyan). (D) Model of the signaling cascade regulated by Ccn2a which promotes cell proliferation and inhibits cell death.

Figure S1

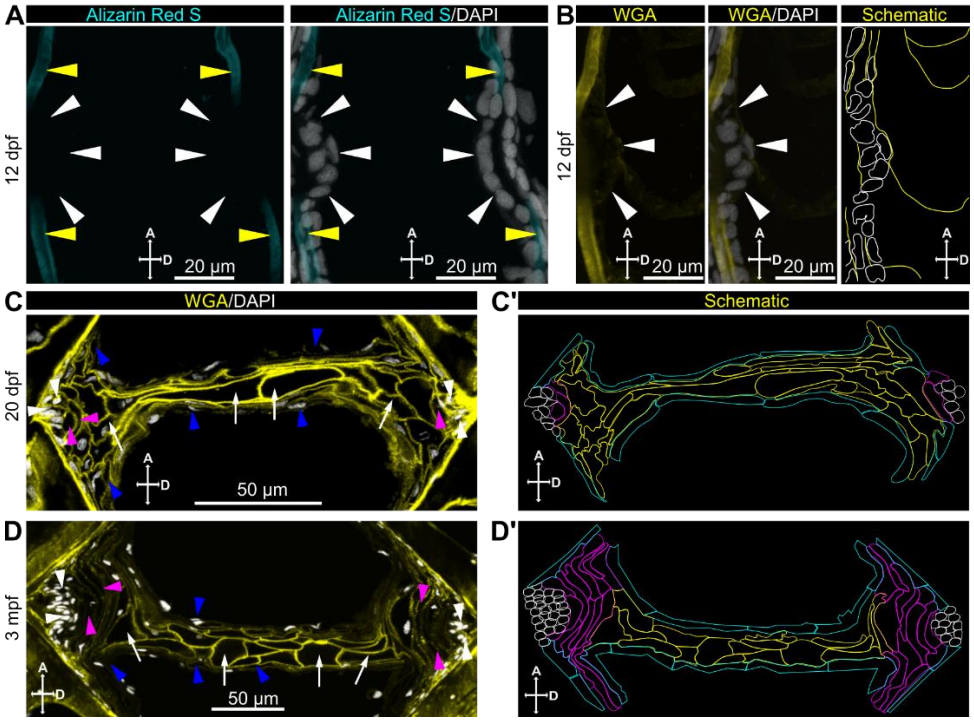

Fig. S1. Morphologically, adult zebrafish intervertebral disc is homologous to the mammalian counterpart. (A) MIPs of confocal images of sagittal sections of IVD stained with Alizarin Red S (cyan; calcified vertebrae) and DAPI (white; nuclei). White and yellow arrowheads indicate vertebrae and sheath cells between two adjacent vertebrae, respectively. (B) MIPs of confocal images of sagittal sections of IVD stained with WGA (yellow; cell membrane) and DAPI (white; nuclei). White arrowheads indicate NSCs protruded into the notochord lumen at the future IVD forming region. The schematic represents the 2nd panel of "B." (C, D) Representative single plane confocal images of sagittal IVD sections stained with WGA (yellow; cell membrane) and DAPI (white; nuclei). White, magenta, and blue arrowheads indicate OAF, IAF, and NSCs, respectively. White arrows indicate NP. (C', D') Schematics of C (C') and D (D') show the cell morphology and cellular organization of the IVDs. White, magenta, yellow, and cyan denote OAF, elongated IAF, large NP, and elongated notochordal sheath cells, respectively. MIP; maximum intensity projection, OAF; outer annulus fibrosus, IAF; inner annulus fibrosus, NP; nucleus pulposus, NSCs; notochordal sheath cells.

Figure S2.

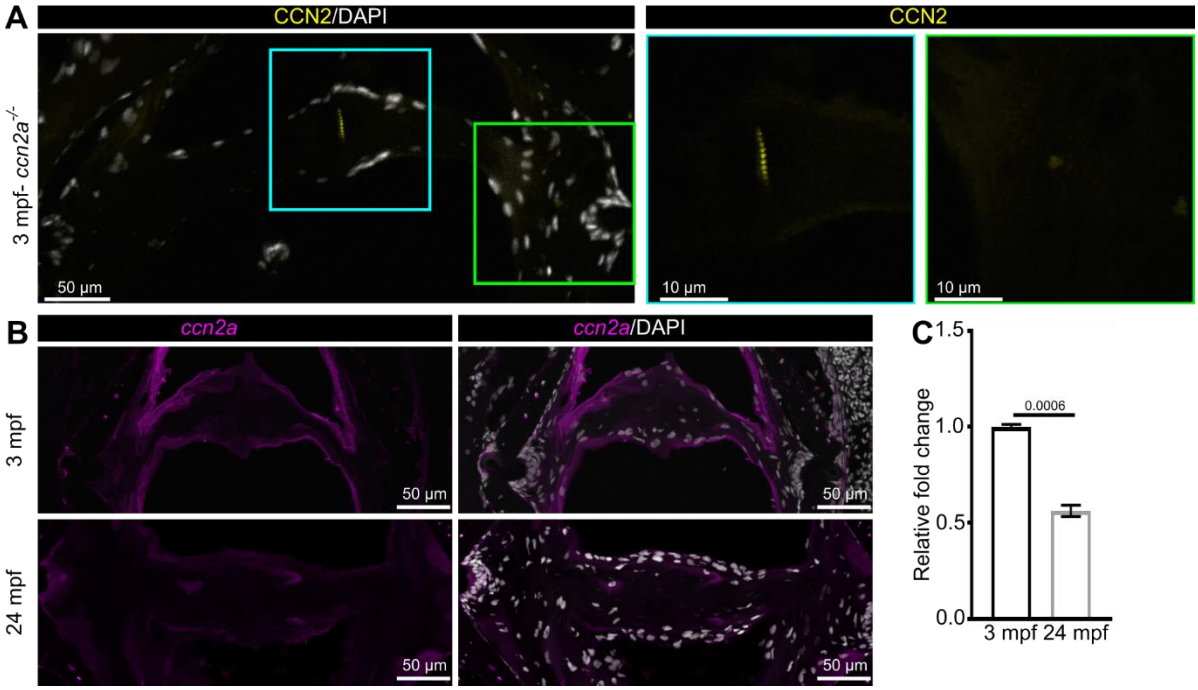

Fig. S2. Decreased *ccn2a* expression in aged zebrafish IVD. (A) *ccn2a*$^{-/-}$ do not show a signal for CCN2 immunostaining. (B) Maximum intensity projections of confocal images of *BACccn2a*:EGFP expression (magenta) in sagittal sections of 3 mpf and 24 mpf IVD (white; nuclei). (C) Quantification of *ccn2a* transcripts in 3 mpf and 24 mpf zebrafish vertebral tissues (n=4). Data are mean ± s.e.m. and each sample represents one animal. Mean Ct values-Table S5.

Figure S3

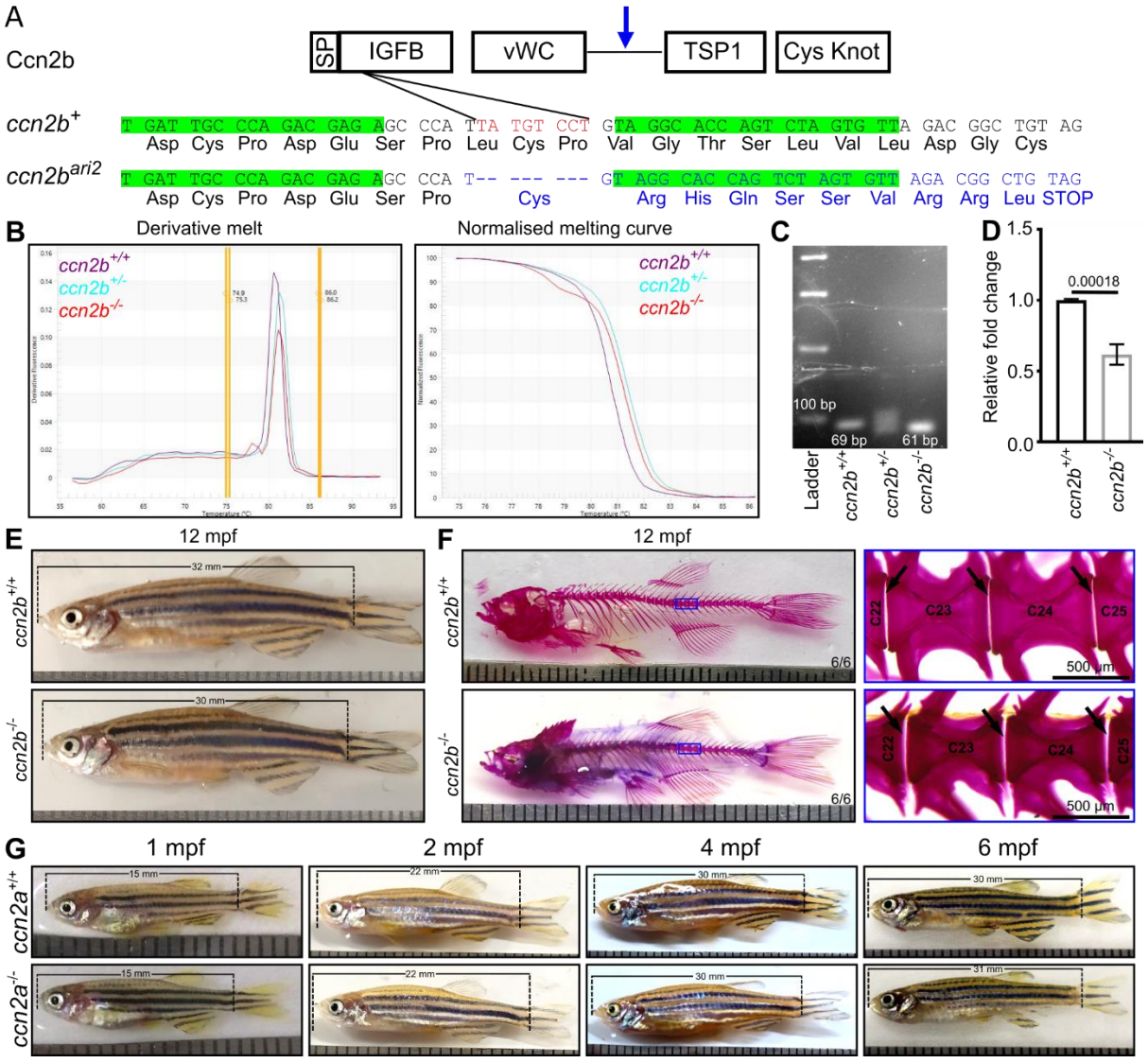

Fig. S3. *ccn2b*$^{-/-}$ and *ccn2a*$^{-/-}$ are adult viable. (A) Diagram shows the domains of Ccn2b protein. Arrow indicates protease domain. Genomic organization of *ccn2b* wild-type (*ccn2b*$^{+}$) and mutant (*ccn2b*^{ari2}) alleles. The left and right arm binding sites of TALEN are highlighted in green. Mutated nucleotides and altered amino acids are shown in blue. (B, C) Genotyping of wild-type, *ccn2b* heterozygous (*ccn2b*$^{+/-}$), and *ccn2b* homozygous (*ccn2b*$^{-/-}$) mutant animals by high-resolution melt curve analysis (HRMA) (B), and semi-qPCR (C). (D) qPCR shows decreased *ccn2b* transcripts in *ccn2b*$^{-/-}$ embryos compared to wild-types. Relative expression was normalized to *ef1α* expression, and the mean expression in wild-type animal was considered 1. Data are mean ± s.e.m. (n=4). Mean Ct values-Table S5. (E) Bright-field

images of 12 mpf live animals. mm; millimeter. (F) Bright-field images of 12 mpf whole-mount Alcian blue and Alizarin Red stained zebrafish. (G) Bright-field images of 1- to 6-mpf live wild-type and *ccn2a*$^{-/-}$ siblings. mm; millimeter. Digits on the images indicate the number of fishes that showed presented phenotypes out of the total number of analyzed fishes. Arrows indicate intervertebral spaces.

Figure S4

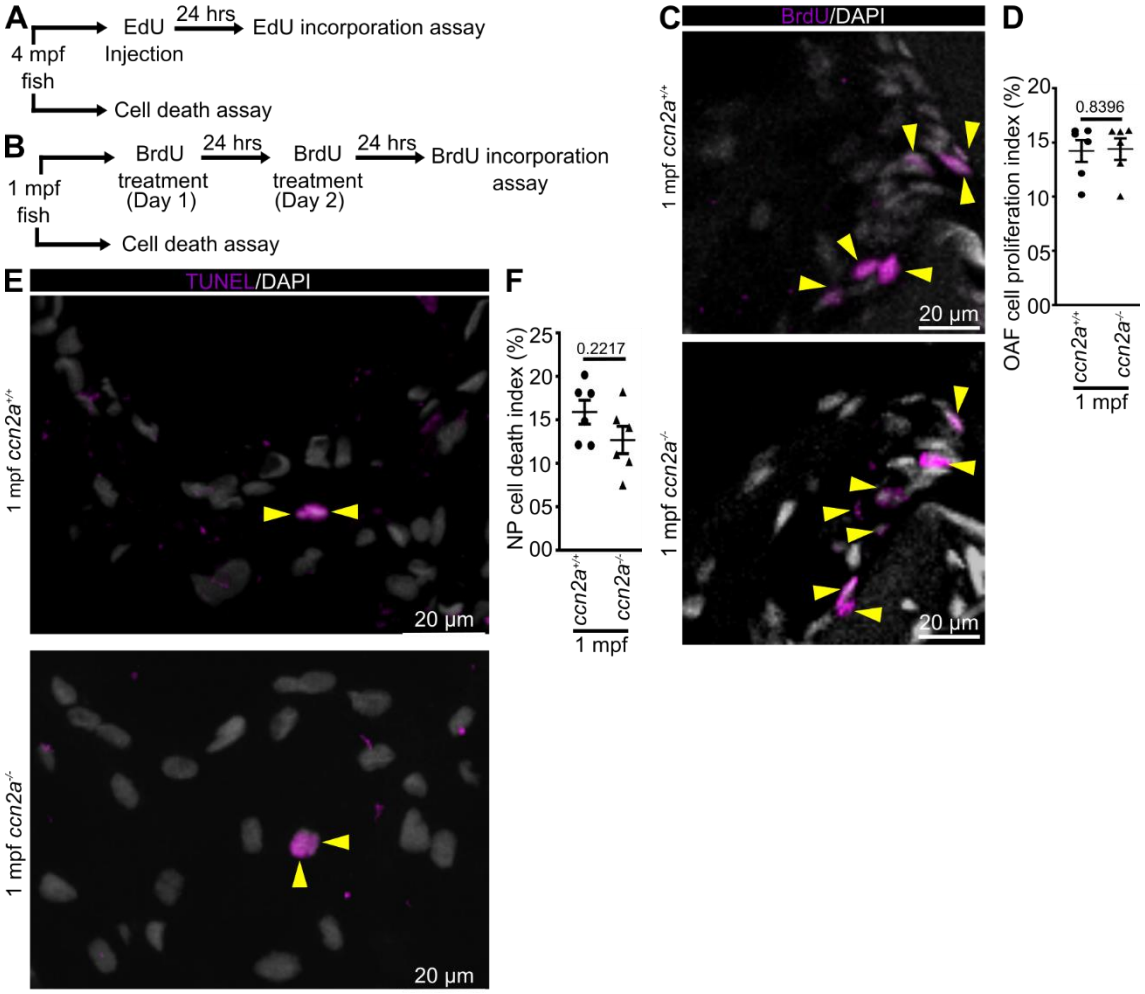

Fig. S4. OAF cell proliferation and NP cell death in *ccn2a*$^{-/-}$ are comparable to wild-type animals at 1 mpf. (A, B) Schematic depiction of experimental procedures. (C) MIPs of confocal images of sagittal IVD sections stained for BrdU (magenta; proliferating cells) and stained with DAPI (white; nuclei). Arrowheads indicate BrdU^{+} OAF cells. (D) Dot plot depicting the percentage of BrdU^{+} OAF cells (n=6). (E) MIPs of confocal images of sagittal IVD sections stained for TUNEL (magenta; dead cells) and stained with DAPI (white; nuclei). Arrowheads indicate TUNEL^{+} NP cells. (F) Dot plot depicting the percentage of TUNEL^{+} NP cells (n=6). Data are mean ± s.e.m. in D and F. MIP; Maximum intensity projection.

Figure S5

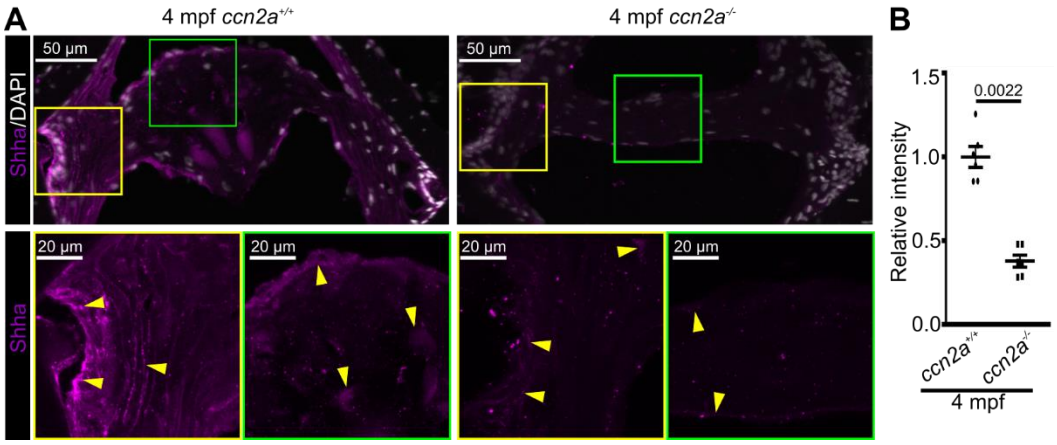

Fig. S5. Shha expression is decreased in *ccn2a*$^{-/-}$ IVDs at 4 mpf. (A) Maximum intensity projections of confocal images of sagittal IVD sections immunostained for Shha (magenta) and stained with nuclei (white, DAPI). Arrowheads indicate Shha expression. (B) Quantification of the relative intensity of Shha in 4 mpf IVDs (n=6). The mean of wild-type control value was set to 1. In B data are mean ± s.e.m.

Figure S6

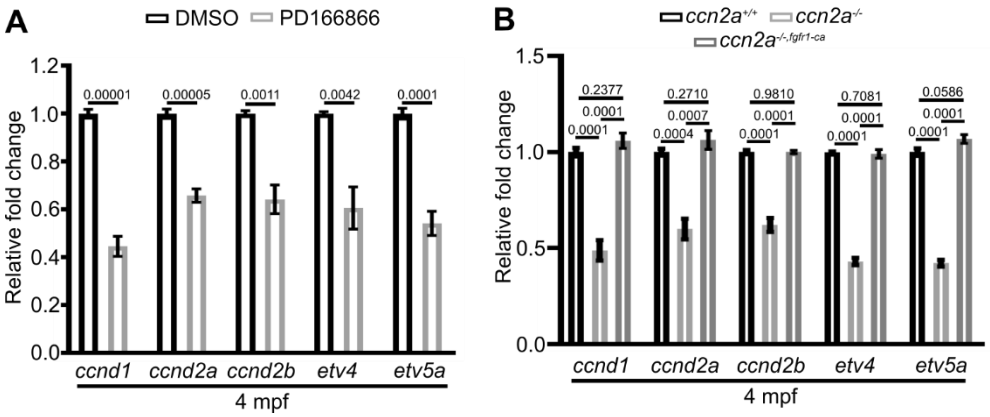

Fig. S6. FGFR1 signaling regulates *ccnd1, ccnd2a, ccnd2b, etv4,* and *etv5a* expression in zebrafish vertebral tissues. (A, B) qPCR analysis of *ccnd1*, *ccnd2a, ccnd2b, etv4*, and *etv5a* in vertebral tissues upon pharmacological inhibition (A) or genetic activation (B) of FGFR1 signaling (n=4). Data are mean ± s.e.m. and each sample represents one animal. Mean Ct values-Table S5.

Figure S7

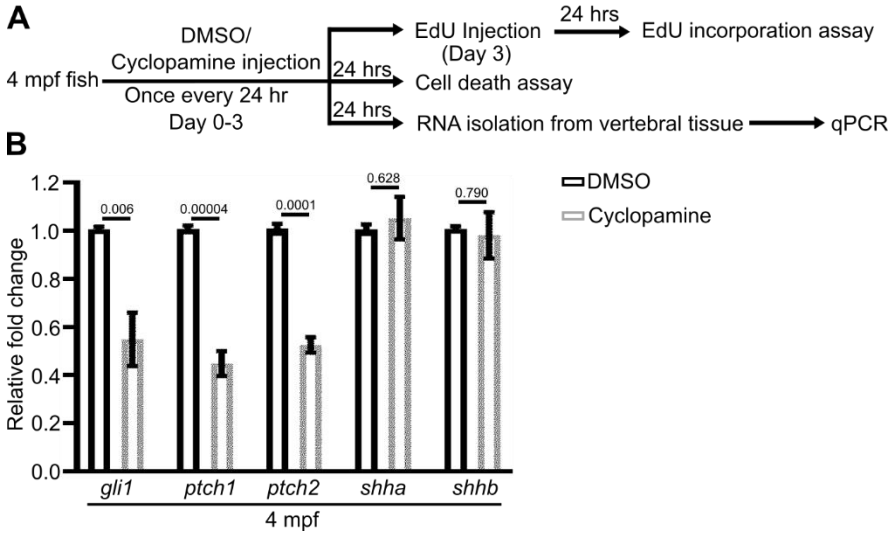

Fig. S7. Cyclopamine inhibits SHH signaling in Zebrafish vertebral tissues. (A) Schematic depiction of experimental procedures. (B) qPCR analysis of *gli1*, *ptch1*, *ptch2*, *shha*, and *shhb* expression in vertebral tissues (n=4). In B data are mean ± s.e.m. Mean Ct values-Table S5.

Figure S8

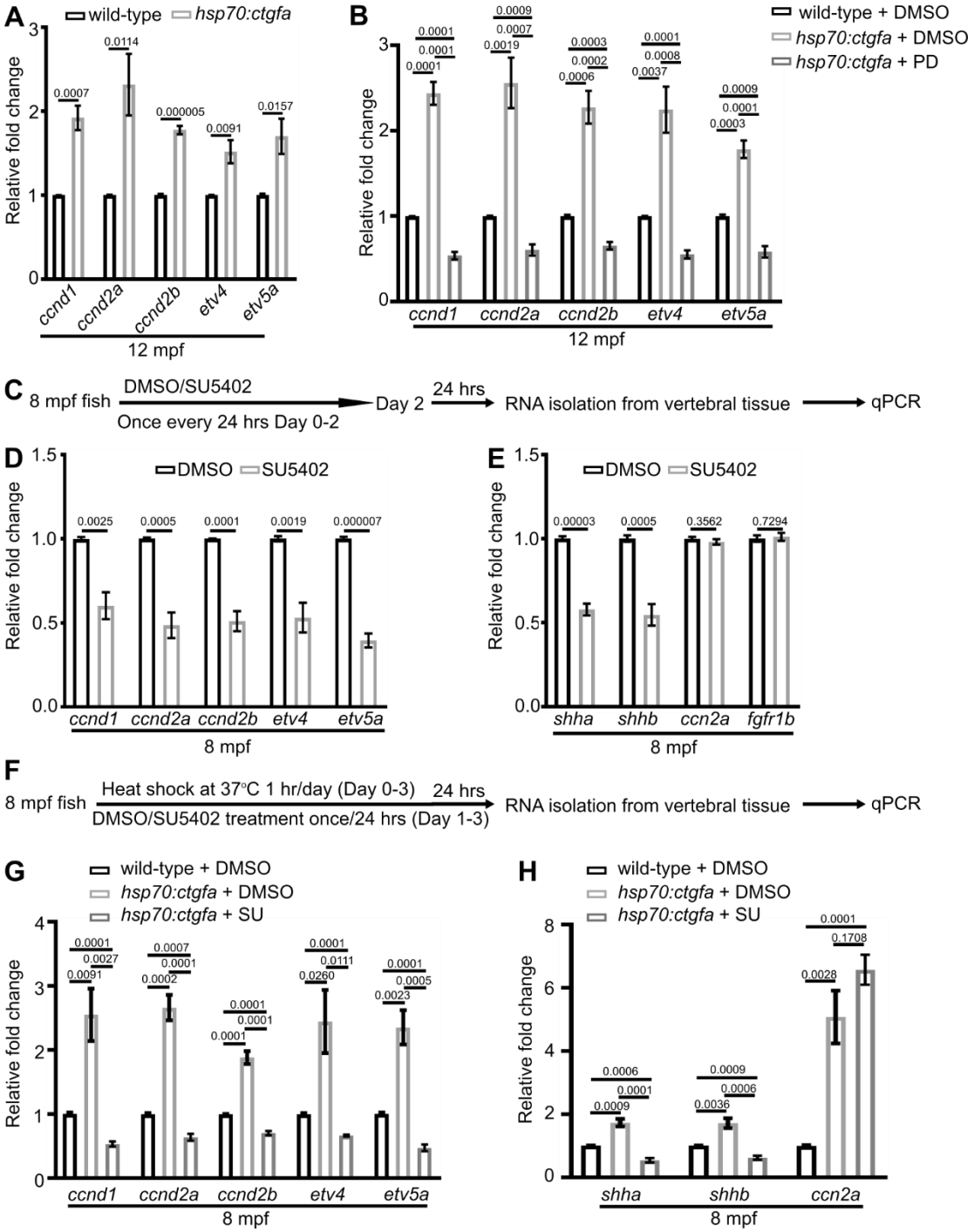

Fig. S8. FGFR1 signaling regulates *shha* and *shhb* expression in adult IVDs. (A) qPCR analysis of FGFR1 signaling target genes in vertebral tissues of 12 mpf wild-type and Ccn2a overexpressing zebrafish (n=4). (B) FGFR1 signaling target gene expression analysis in vertebral tissues of 12 mpf wild-type and Ccn2a overexpressing zebrafish treated with DMSO or PD166866 (n=4). (C) Schematic depiction of experimental procedures. (D, E) qPCR

analysis of FGFR1 signaling target genes (D) and *shha*, *shhb*, *ccn2a*, and *fgfr1b* (E) in vertebral tissues of 8 mpf zebrafish treated with DMSO or SU5402 (n=4). (F) Schematic depiction of experimental procedures. (G, H) qPCR analysis of FGFR1 signaling target genes (G) and *shha*, *shhb*, and *ccn2a* (H) in vertebral tissues of 8 mpf wild-type and Ccn2a overexpressing zebrafish treated with DMSO or SU5402 (n=4). In A, B, D, E, G, and H, data are mean ± s.e.m. and each sample represents one animal. Mean Ct values-Table S5.

Figure S9

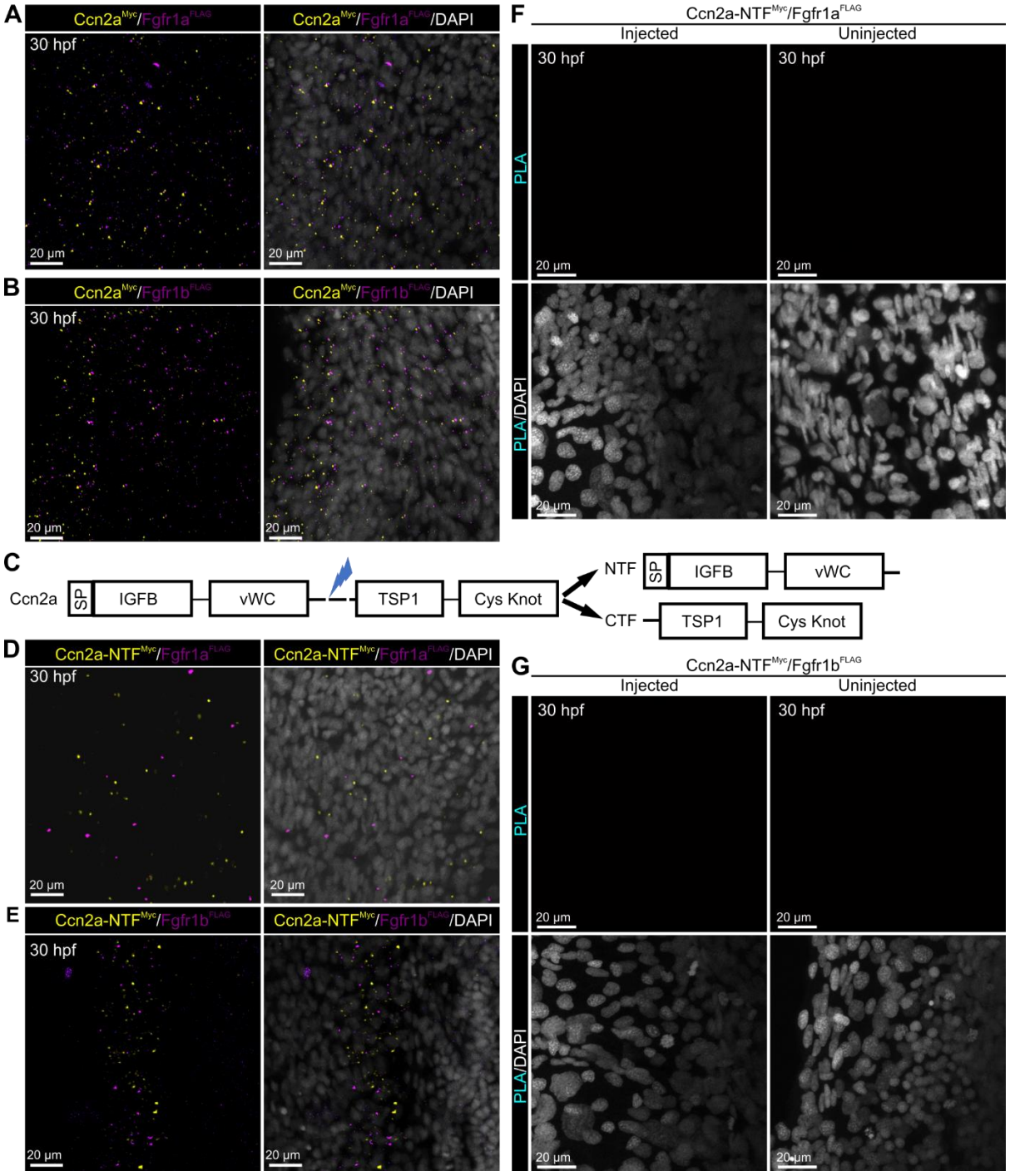

Fig. S9. N-terminal fragment of Ccn2a does not interact with Fgfr1a and Fgfr1b. (A) MIPs of confocal images of whole-mount 30 hpf embryos stained for Myc-tagged Ccn2a (yellow) and FLAG-tagged-Fgfr1a (magenta) and stained with DAPI (white, nuclei). (B) MIPs of confocal images of whole-mount 30 hpf embryos stained for Myc-tagged Ccn2a (yellow) and FLAG-tagged-Fgfr1b (magenta) and stained with DAPI (white, nuclei). (C)

Diagram shows the structure of Ccn2a full length protein, N- terminal fragment (NTF), and C-terminal fragment (CTF). (D) MIPs of confocal images of whole-mount 30 hpf embryos stained for Myc-tagged Ccn2a-NTF (yellow) and FLAG-tagged- Fgfr1a (magenta) and stained with DAPI (white, nuclei). (E) MIPs of confocal images of whole-mount 30 hpf embryos stained for Myc-tagged Ccn2a-NTF (yellow) and FLAG-tagged- Fgfr1b (magenta) and stained with DAPI (white, nuclei). (F, G) Representative single plane optical sections of whole-mount 30 hpf embryos stained for proximity detection (cyan, interacting protein complex) and stained with DAPI (white, nuclei). No spots of the proximity of C-terminal Myc-tagged Ccn2a-NTF and C-terminal FLAG-tagged- Fgfr1a (F) or Fgfr1b (G) were detected. MIP, maximum intensity projection; PLA, proximity ligation assay; Ccn2a-NTF, N-terminal fragment of Ccn2a.

Figure S10

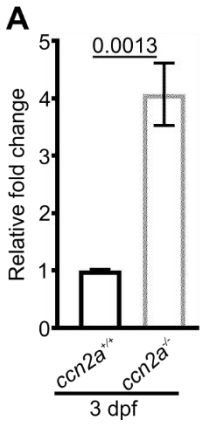

Fig. S10. Increased *ccn2b* expression in *ccn2a*$^{-/-}$ embryos. Quantitative analysis of the *ccn2b* expression in 3 dpf wild-type and *ccn2a*$^{-/-}$ embryos (n=4). Data are mean ± s.e.m. Each sample represents a pool of 30 embryos. Mean Ct values-Table S5.

Table S1. Oligonucleotides used for qPCR

Sr. No.	Gene Name	Sequence (5'→ 3')	
		Forward	Reverse
1	*bmp2b*	GCTCGAACTGTAGGCGACAT	AATGGCATGGTTGGTGGAGT
2	*bmp4*	CGCCTCTGCGATTCGTTTTT	GATCTGGGTCTGAGAAGGCG
3	*ccn2a*	GGTGTACCGCAGTGGAGAGT	CTACAGCACCGTCCAGACAC
4	*ccn2b*	CAGGACTGCTCTCAGCCCT	CAGCAGCTACAGCCGTCTAA
5	*ccnd1*	AAAGCACCGACAGTTGCCTC	CCAGCAGGGACTCGATCTGTT
6	*ccnd2a*	AGAGTTTGCTGACCATCGAAGAGA	GTTGCCACCATCCTCCGCAT
7	*ccnd2b*	CCTCCCTCCATGATCGCCAC	GCTCCATCAGATTGTCGCCC
8	*col1a1a*	TATTGGTGGTCAGCGTGGTA	TCCTGGAGTACCCTCACGAC
9	*col1a2*	CTGGCATGAAGGGACACAG	GGGGTTCCATTTGATCCAG
10	*col2a1a*	GATGTGGAGATCAGAGCAGAGGG	CATGATGGGCAGTCTGGATGTCT
11	*col2a1b*	ACGGATGCAAGAAACACACAGGA	TCCACAGGGGCAATGTCCACAA
12	*col9a1a*	AAAACCAGGCCGAGCACCAA	CTCGGGCCTTGTCAGACTGG
13	*col9a2*	CAGCGCCGACTTTCAGTGTC	CCAACACCCCAGAACGACCT
14	*col9a3*	CCCGGAAAACCAGGACCGAT	TCCCTGATGTGCTGCTCACT
15	*col11a1a*	GAGAGGCCAAGGTGGTCCC	CCTGCAGAACCAGGACGAG
16	*col11a1b*	CAAAAGGCCCGGTTGTGTCG	CCGGAGCGTCCTGTCAATCC
17	*col11a2*	GATATTCGGAAGAAGCGGAGG	CGCAAAACATCTACTGGATCTG
18	*col12a1a*	CAATCCAGCAACACAAGTGG	AACCGATTTAGCCGCTTT
19	*col12a1b*	GTGGCTCTCTTTACACTCGC	ATTATCAAACTGCTCGCTGC
20	*ef1α*	CTGGAGGCCAGCTCAAACAT	CAAGAAGAGTAGTACCGCTAGC
21	*etv4*	ACACTTACGAACCTGATGTGCCT	CTGGCACAACACGGGAATCA
22	*etv5a*	AGCCTTGCCTTCCATTCCCA	TTTGGCGATGGTACGGTGGT
23	*fn1a*	GGTCATCGTCCAGTCCAG	ATCCACTGAATATGGGTGTT
24	*fn1b*	TGGAAATGTGATGCTATTGA	GGCCAATCTGGTAGAACACC
25	*fgfr1a*	GTCTATAAAGCCGTTCCCCC	CGGTCCCCACCATCACACAG
26	*fgfr1b*	GTTGTTAAAGCCCCCACTGC	GGTGGCGATTCCTACCATGAGG
27	*fgfr2*	AAGAGCCTCCAACCAAAAAC	TCATCTGCCCCGGACAGCG
28	*fgfr3*	GTCCCCAGAGCCCACAGACT	GGAGGAAGTCTTGCGGCGTG
29	*fgfr4*	CCCAGGGCAAAAGATATCAG	GGTGGAGCTTACACACCAGCTT
30	*gli1*	AACACAAGACGTGCCAGCGA	CAGTGCATTCCGGCGACTCA
31	*ptch1*	TTCGCCCAGCACACCCAAAT	GAGATGTGGGAATGGGGCTC
32	*ptch2*	CTTTAATGCCGCCACCACGC	GGGATGTTGGATCGGGTCTCT
33	*shha*	GCTTTTGACGAGAGTGCTGCT	TAAGGTCTTCTCCGCGACAT
34	*shhb*	AACGCTGACAGGCTGATGACCA	CAGTGACGCGCAGTTTCACGC
35	*tgfβ1a*	GTTGGTTTGCTTGGTGCTGA	ATCTTCTGTCCGTCGTCGTC
36	*tgfβ2*	TGAACTTGTACGTCTTGAGCC	GATCTCAGGAGGACTGCTCA
37	*tgfβ3*	AAAGGACTGCTGTTTGTTCTG	ATCCCTGGTGCTGTTGTAGA

Table S2. Oligonucleotides used for RNA probe synthesis

Sr. No.	Gene Name	Sequence (5'→ 3')	
		Forward	Reverse
1	*ccn2a*	TTTCCGGCTGTACCACTACC	CTGCCAATCAGTGACATTGG
2	*ccn2b*	GAACCCCAAAAAGCCAGAGT	CAGTGCCCACTTCATGTCAA
3	*fgfr1a*	GTCTATAAAGCCGTTCCCCC	TGTCTCGTTGCACCTCCCAG
4	*fgfr1b*	GTTGTTAAAGCCCCCACTGC	TAGCCTCTCTCTGGACACTT
5	*shha*	GCTTTTGACGAGAGTGCTGCT	CAGCTAGGCGAGACAGTGTC
6	*shhb*	AACGCTGACAGGCTGATGACCA	TCTCGTTGTCGGATCGTGGTCT

Table S3. Oligonucleotides used for mRNA synthesis.

Sr. No.	Gene Name	Orientation	Sequence
For p3XFLAG-CMV-14			
1	*fgfr1a*	Forward	ATGAAGATGATGATGATAAT
		Reverse	GCGCTTTTTAAAGGCCACTC
2	*fgfr1b*	Forward	ATGATCTTTCTGTCAGCCGC
		Reverse	GCGTTTTTTGAAGGAGCGCA
For pCMV-Myc-C			
1	*ccn2a*	Forward	ATGTTTTCTGGAATGACTCA
		Reverse	CCGCCATGTCGCCAACCATCT
2	*ccn2a*-NTF	Forward	ATGTTTTCTGGAATGACTCA
		Reverse	CACACACCCACTCCTCGCAGC
For pCS2+			
1	*ccn2a*	Forward	ATGTTTTCTGGAATGACTCA
2	*ccn2a*-NTF	Forward	ATGTTTTCTGGAATGACTCA
3	myc	Reverse	TTACAGGTCCTCCTCTGAGA
4	*fgfr1a*	Forward	ATGAAGATGATGATGATAAT
5	*fgfr1b*	Forward	ATGATCTTTCTGTCAGCCGC
6	FLAG	Reverse	CTACTTGTCATCGTCATCCTTGT

Table S4. Oligonucleotides used for genotyping

Sr. No.	Gene Name	Sequence (5'→ 3')	
		Forward	Reverse
1	*ccn2a*	GGTGTACCGCAGTGGAGAGT	CTACAGCACCGTCCAGACAC
2	*ccn2b*	TGATTGCCCAGACGAGAGCCC	CAGCAGCTACAGCCGTCTAA

Table S5. Mean of ct values used for gene expression analyses.

Click here to download Table S5